Politecnico di Torino

Corso di Laurea Magistrale in
Mechanical Engineering
a.a. 2021/2022

# Experimental analysis of the mechanical properties of aluminum tailor welded blanks

**Relatori**
Prof.ssa Raffaella Sesana
Prof.ssa Manuela De Maddis

**Candidato**
Dario Basile

*Ai miei Genitori, a Valeria e Corrado,*

*Grazie di tutto.*

# Abastract

Nowadays the of the reduction of $CO_2$ emissions and the decrease in energy consumption are the aims for different industries around the world. In order to satisfy increasingly restrictive regulations, the automobile industry is constantly looking for innovative techniques to produce lighter automobiles, more efficient and less polluting. One of the latest technologies designed, and still developing, is that of Tailor Welded Blanks. TWBs are combination of multiple metal sheets with various thicknesses and/or strengths are welded together using high speed weld along their edges. Over the years, the advantages of using aluminium in this technology have been discovered, thanks to its low density, high corrosion resistance, and good weldability. However, its use is limited by low formability when complex geometries come into play.

This study will investigate the mechanical and microstructural properties of EN AW5754 and EN AW6016 aluminium tailor blanks obtained from a Nd:YAG laser welding process, having a variable thickness. The research is carried out in collaboration with the company CO. ST. AT. s.r.l. of Piobesi Torinese (TO), interested in the to the improvement of this process. In particular, the influence of welding parameters on tensile strength and joint formability will be studied, analyzing a L9 Taguchi model.

# Contents

# List of Figures

# List of Tables

# Chapter 1

# Introduction

## 1.1 Tailored Blanks

The protection of the environment and the decrease in energy consumption are now general aims for different industries around the world [46]. In order to satisfy increasingly restrictive regulations, the automobile industry is constantly looking for innovative techniques to produce lighter automobiles, more efficient and less polluting. One of the latest technologies designed, and still developing, is that of Tailor Blank: sheet metal panels composed of elements of different materials and/or thicknesses welded together. Four different types of tailor blank can be distinguished (figure 1.1):

- *Tailor Welded Blanks (TWB)*: Sheet metal panels with different characteristics are joined by a welding process, typically laser (but continuous roller, high frequency, electron beam, induction or friction stir welding seams can also be found);

- *Patchwork Blanks*: The plate is reinforced locally by the addition of a second panel;

- *Tailor Rolled Blanks*: A continuous variation of sheet thickness is created by a rolling process;

- *Tailor Heat Treated Blanks*: The properties of the material are modified in specific areas by local heat treatments.

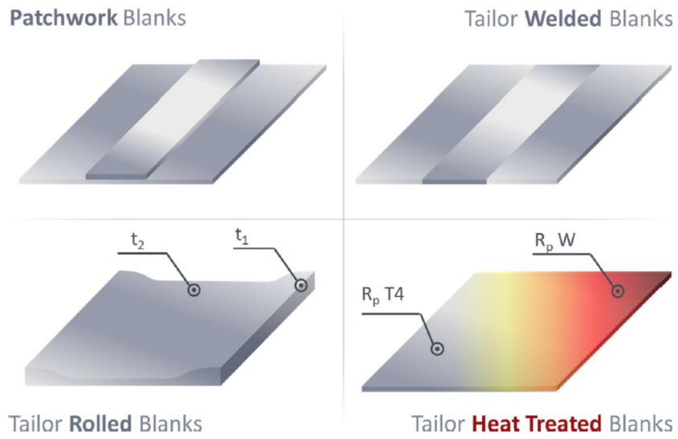


Figure 1.1: Classification of tailored blanks.

In this study only *Tailor Welded Blanks (TWB)* will be considered, focusing on laser welding process on sheets of different thickness. TWBs are combination of multiple metal sheets with various thicknesses and/or strengths are welded together using high speed weld along their edges prior to the forming process (see figure 1.2) [36].

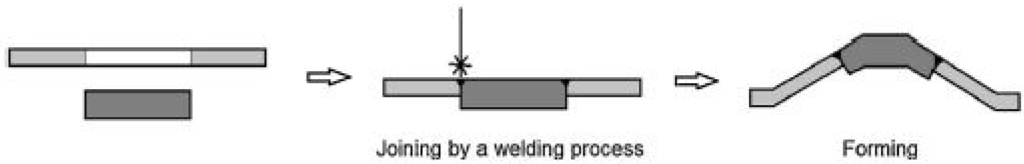


Figure 1.2: Principle of tailor welded blanks

The most common application of TWBs is in the automotive sector, where they are used for the realization of components belonging to the body-in-white of the vehicle, as schematized in 1.4.

The term body-in-white means all the structural parts of a car assembled together before the engine and transmissions, body parts, bonnets, doors, bumpers, wheel arches, interiors, windows and systems are fitted, and is essentially the ”core” of the vehicle (fig. 1.3). The main advantage of using TWBs lies in the possibility of reinforcing the component with a greater thickness only in areas where greater strength or stiffness is required (as in the vicinity of the hinges of the doors), and to maintain a lower

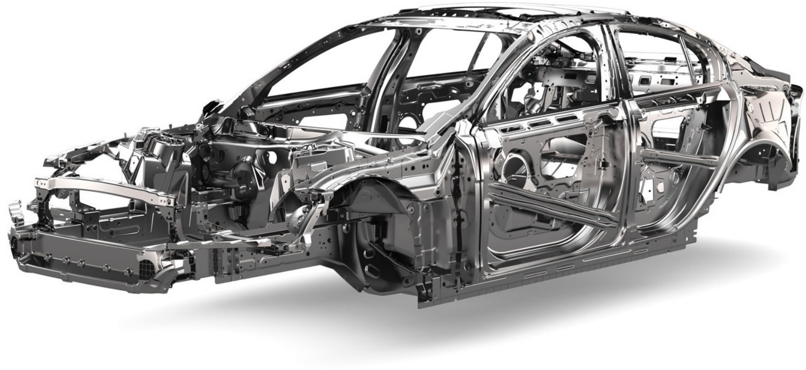

Figure 1.3: The BiW of a car

thickness in the rest of the component, resulting in a reduction in the weight and fuel consumption of the motor vehicle [25].

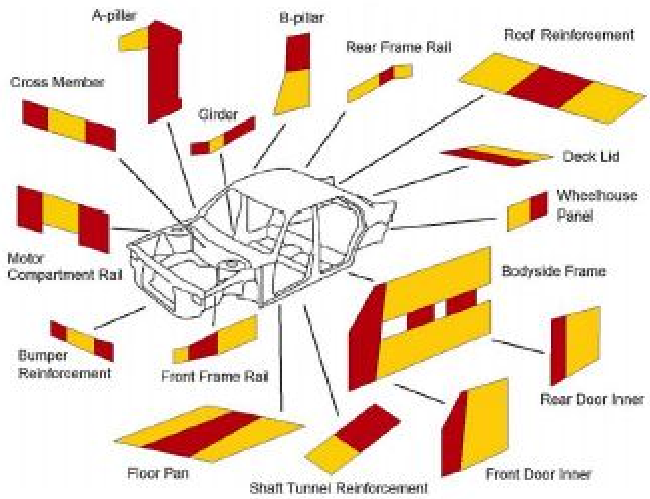


Figure 1.4: Application of TWB in the BiW

The statistics shows that the 10% decrease in weight of vehicle leads to reduction in fuel consumption around a 6–8% [51] and it has been estimated that replacing steel with aluminum in body-in-white can result in weight savings as high as 55% [18]. It would be wrong to think that using these elements leads to weaker cars, indeed the safety performance in the event of an accident is also improved, as components with high stiffness zones (safety cells) and more deformable zones, capable of absorbing the energy of the impact, can be produced [54, 25].

## 1.2 Aluminum alloys

Aluminum is the the most abundant metal present in the crust of the earth [29]. It is obtained from bauxite containing around 50% of hydrated alumina (aluminium oxide) as well as iron oxides, silica and titania. Pure Aluminium (i.e. with a minimum aluminum content of 99.50%) is a silvery gray metal with a face-centered cubic crystalline structure. Its density and its melting temperature are respectively equal to 2700 kg/m$^3$ and 660°C [31]. The main properties of pure aluminum, which have made it industrially important, are:

- low density;
- good electrical and thermal conductivity;
- high deformability
- good corrosion resistance in neutral environments with pH = 4÷8
- good weldability: due to the strong reactivity of aluminum with oxygen, it is necessary to use protective atmospheres in order to isolate the weld joint from the surrounding environment; the main techniques used are TIG - Tungsten Inert Gas and MIG - Metal Inert Gas);
- high reflectance (reflectance refers to the portion of incident light that a given surface is capable of reflecting);

The mechanical properties of pure aluminum, in the annealed state, are quite low (tab. 1.1).

The poor mechanical properties of pure aluminum have always prevented its wide use in industry, where instead its alloys are widely used. The main alloying elements used in commercial alloys are copper, manganese, silicon, zinc and magnesium; the effects of these elements on aluminum properties are synthetically listed in figure 1.5.

The addition of alloying elements allows a considerable improvement in tensile strength, which can exceed that of mild steels, making aluminum alloys suitable for

| | |
|---|---|
| Ultimate tensile strength, $R_m$ | 60÷100 MPa |
| Yielding stress, $R_{p0.2}$ | 30÷50 MPa |
| Hardness | 15÷25 HB |
| Young's modulus, E | ≈ 70.000 MPa |
| Percent elongation before break | $>$ 40% |

Table 1.1: Mechanical properties of Pure Aluminum

| | Cu | Mn | Si | Mg | Zn |
|---|---|---|---|---|---|
| Proprietà meccaniche | ↑↑ | ↑ | ↑ | ↑ | ↑↑ |
| Deformabilità a freddo | ↓ | ↑ | ↓ | ↓ | ↓ |
| Resistenza a corrosione | ↓ | ↑ | = | ↑ | = |
| Saldabilità | ↓ | ↑ | = | ↑ | ↓ |

Figure 1.5: Effect of major alloying elements on mechanical strength, cold deformability, corrosion resistance, and weldability of pure aluminum

structural applications. This consideration is even more true if we examine the specific mechanical properties, i.e. related to density ($\sigma/\rho$), the real reference parameter for all applications where there are problems of weight containment. In fact, aluminum alloys show very high values of specific tensile strength, even higher than those of high-strength steels (see fig. 1.6).

Aluminum alloys are usually divided into two categories:

- Wrought alloys;
- Cast alloys.

The alloys object of this study will be the wrought alloys, these are so called because their use takes place in the state of semi-finished cold plastically deformed. These alloys are designated by means of a four-digit number, which allows to identify the chemical composition of the alloy.

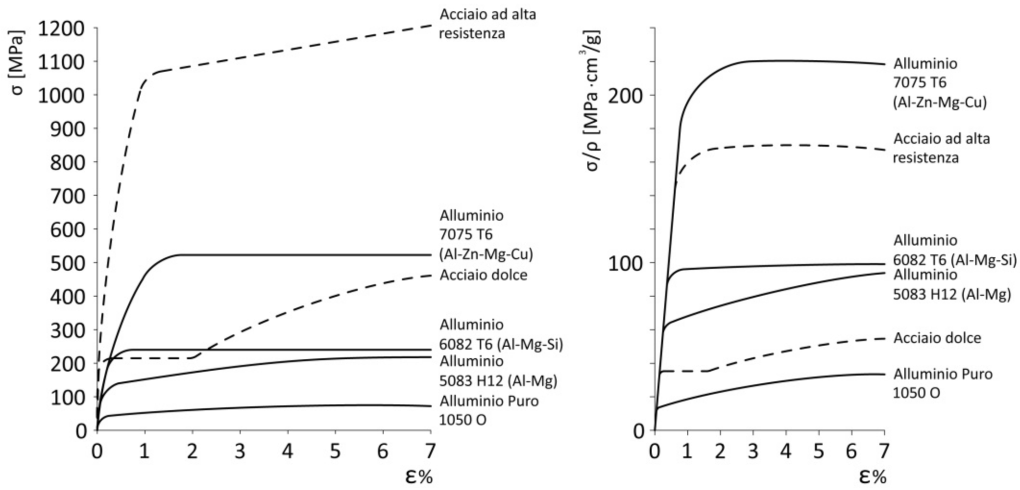


Figure 1.6: Tensile curves - and $\sigma/\rho$ tensile curves - for some aluminum alloys and for a mild steel and a high strength steel
(*M. Conserva, F. Bonollo, G. Donzelli, Alluminio - Manuale degli impieghi*)

The first digit indicates the family of alloys as follows:

- 1xxx: pure aluminum (containing at least 99.0% aluminum);
- 2xxx: aluminum-copper alloys;
- 3xxx: aluminum alloys - manganese;
- 4xxx: aluminum alloys - silicon;
- 5xxx: aluminum alloys - magnesium;
- 6xxx: aluminium alloys - magnesium - silicon;
- 7xxx: aluminum alloys - zinc - magnesium;
- 8xxx: aluminium alloys containing elements other than those previously listed.

The second digit is zero if the alloy contains elements that conform to its family, while it is non-zero if there are variations from the base alloy.

The third and fourth digits:

- in non-alloyed aluminum (1xxx) indicates the minimum percentage of aluminum; The number refers to decimal places, for example 1050 indicates 99.50% pure aluminum;

- in aluminum alloys indicate a progressive number that uniquely defines the alloy within the family to which it belongs.

This designation, born in the United States by the Aluminum Association, is currently used in Europe. In the USA the four digits are preceded by the letters AA (Aluminum Association) while in Europe AA is replaced by EN AW where EN stands for ”Europeén Normalisation” and AW for ”Aluminum Wrought”, English terminology to indicate semi-finished products (”Wrought”) in aluminum alloy. For example, the two acronyms below are representative of the same alloy:

- AA 6060;

- EN AW 6060.

Figures 1.7, 1.8 and 1.9 shows some characteristic properties of wrought aluminum alloys.

Plastic deformation alloys are further divided into two categories on the basis of the metallurgical mechanism used for their strengthening. A distinction is made between work hardening alloys and heat-treated alloys.

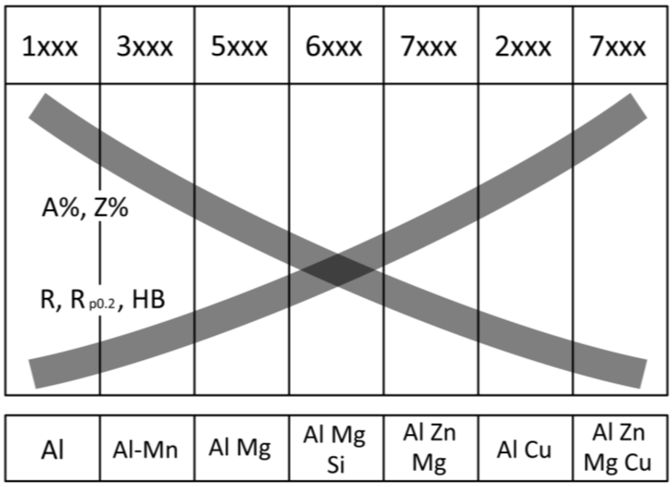


Figure 1.7: Qualitative trend of mechanical properties as a function of different families of wrought aluminum alloys
(*M. Conserva, F. Bonollo, G. Donzelli, Alluminio - Manuale degli impieghi*)

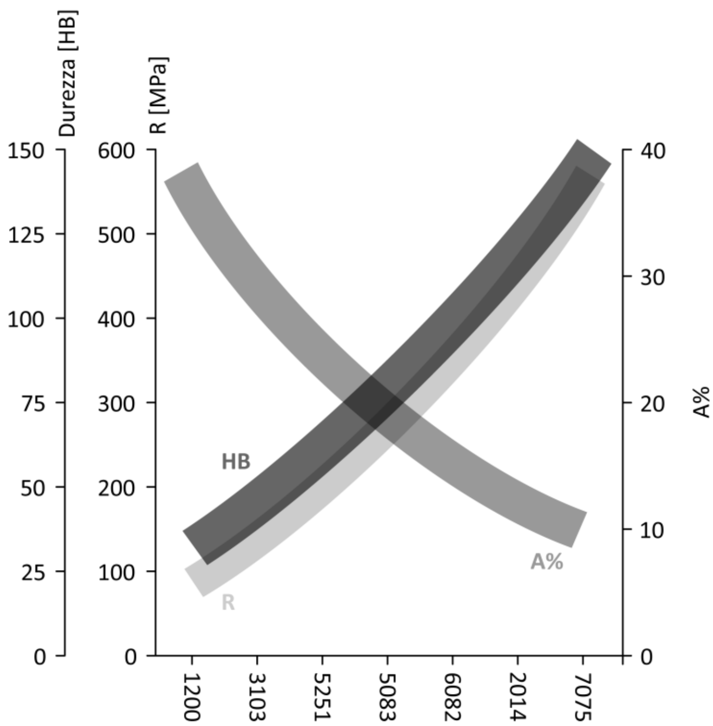


Figure 1.8: Trend of ultimate tensile strength (R), Brinell hardness and percent elongation at break (A%) for wrought aluminum alloys, belonging to 1000, 2000, 3000, 5000, 6000 and 7000 series.

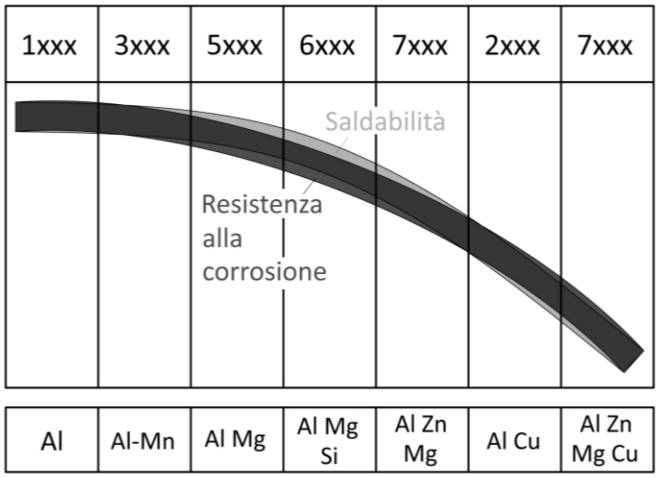


Figure 1.9: Qualitative trend of weldability (in italian: saldabilità) and corrosion resistance as a function of different families of wrought aluminum alloys (*M. Conserva, F. Bonollo, G. Donzelli, Alluminio - Manuale degli impieghi*)

### 1.2.1 Work-Hardened Aluminum alloys

They belong to this category of wrought aluminum alloys:

- 1xxx (Pure Aluminum)
- 3xxx (Aluminum - Manganese)
- 4xxx (Aluminum - Silicon)
- 5xxx (Aluminum - Magnesium)
- 8xxx (only some, such as aluminum-iron alloys and aluminum-nickel alloys)

The common characteristic of these alloys is that their mechanical resistance can be improved only by work hardening, that is subjecting the material to a cold plastic deformation. It is not possible to apply heat treatments to these alloys, with the exception of annealing, which has the purpose of reducing or eliminating the residual stresses present in the material following plastic deformation. If carried out at lower temperatures (200°C ÷ 250°C) it leads to only one crystalline rearrangement, while at higher temperatures (350°C ÷ 400°C) it causes a partial or complete recrystallization of the material. Cooling must take place slowly, and can be carried out in an oven or in air. The material in the annealed state will be characterized by higher mechanical strength and lower cold deformability. Following annealing, however, some of the cold deformability is recovered at the cost of a reduction in mechanical strength. The heat treatment status of work hardening alloys is indicated by a letter placed after the four digits of the identification code. The codes that can be found are as follows:

- F: as manufactured; minimum mechanical strength values are not guaranteed;
- O: annealed; it allows to obtain the minimum hardness value required for a given type of alloy;
- H: strain hardened after annealing.

### 1.2.2 Heat-Treated Aluminum alloys

Alloys belonging to the following series are heat treated (also called quenched and tempered or aged):

- 2xxx (aluminum-copper);
- 6xxx (aluminum-magnesium-silicon);
- 7xxx (aluminum-zinc-magnesium);
- 8xxx (only some, such as aluminum-lithium alloys).

These aluminium alloys are used for the realization of many semi-finished products, such as rolled, forged, drawn and extruded products: they are initially hot plastically deformed and then undergo a heat treatment to improve their mechanical resistance. The typical thermal cycle involves the following steps:

1. Solubilization: the material is heated and maintained at a temperature in the range of 450°C ÷ 550°C, which allows for solubilization in the aluminum matrix of most of the alloying elements.

2. Tempering: the material is rapidly cooled in water to room temperature. A solid solution over-saturated with alloying elements is obtained, which do not have time to form the phases normally provided for in the state diagram.

3. Aging: the material is heated and maintained at a lower temperature, in the range of 150 °C ÷ 200 °C. The result is the precipitation of intermetallic compounds (such as $CuAl_2$, $Al_2CuMg$, $Mg_2Si$, $MgZn_2$, $Al_3Li$) that are dispersed in the aluminum matrix in a fine and homogeneous manner. The alloys of the 2xxx, 6xxx and 7xxx series (and some 8xxx) can undergo this treatment since they are the only ones containing the elements (Cu, Mg, Zn and Li) capable of forming the intermetallic compounds that cause strengthening. Aging carried out in this way is called ”artificial”, but it can also be ”natural”, if done at room temperature. Usually, the combination of the first two phases is called ”solution hardening” or ”structural hardening”.

Usually, the combination of the first two steps is called ”solution hardening” or ”structural hardening”. In this case, the state of heat treatment of the alloy is indicated by the letter T and a digit from 1 to 10 which are placed as a suffix to the standard alloy designation. Some examples of codes are as follows:

- T3: solubilization, cold deformation, and natural aging (deformation facilitates nucleation of precipitates);
- T4: solubilization and natural aging;
- T6: solubilization and artificial aging [31];

### 1.2.3 EN AW5754 Aluminum Alloy

The first alloy covered by this study is the EN AW5754, a work hardening Aluminum Alloy having magnesium as its main binding element. Its chemical composition is shown in the table 1.2.

| **Al** | **Mg** | **Si** | **Mn** | **Fe** | **Cr** | **Cu** | **Zn** | **Ti** |
|---|---|---|---|---|---|---|---|---|
| Bal. | 2.6-3.6 | $\leq$0.4 | $\leq$0.5 | $\leq$0.4 | $\leq$0.3 | $\leq$0.1 | $\leq$0.2 | $\leq$0.15 |

Table 1.2: Chemical composition of the 5754 aluminium alloy (% wt).

Figure 1.10 is an optical micrograph of 5754 alloy in an unprocessed state [49]. This figure shows a typical wrought microstructure built of equiaxed grains. According to *Cabibbo (2019)* [9], the 5754 alloy matrixconsist of a Mg in Al solid solution with fine dispersoids of $Mg_2Si$ and $Al_6Mn$ phases.

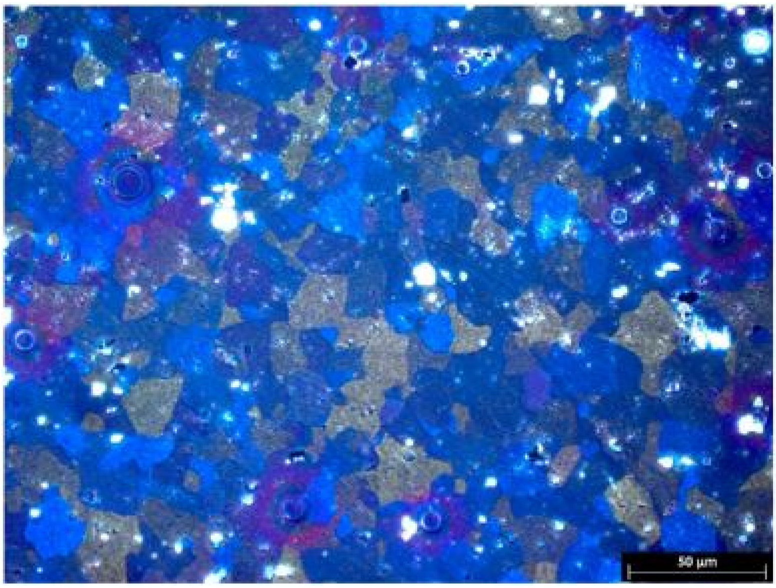


Figure 1.10: Microstructure of the 5754 aluminum alloy in an initial state

As the magnesium content increases (the maximum quantity, in commercial alloys, is 5%), the strength increase, but cold deformability and ductility are progressively reduced. For this reason, extruded profiles in 5xxx series alloys have simple shapes.

The 5xxx series alloys have the following characteristics:

- good deformability;
- good corrosion resistance;
- good weldability;

The alloys of the 5xxx series also have a good mechanical resistance, increasing with the percentage of magnesium (annealed condition).

| | |
|---|---|
| Ultimate tensile strength, $R_m$ | 120÷280 MPa |
| Yielding stress, $R_{p0.2}$ | 60÷130 MPa |
| Hardness | 45÷75 HB |
| Young's modulus, E | 70.000 MPa |
| Percent elongation before break | 10÷25% |

Table 1.3: Mechanical properties of 5xxx series Aluminum Alloy

### 1.2.4 EN AW6016 Aluminum Alloy

Another alloy covered by this study is the EN AW6016 T4, the chemical composition of which is shown in table 1.4. 6xxx series aluminum alloys are considered as the most promising candidate materials for automobile body panels because of the characters of high strength, high formability and excellent corrosion resistance [55].

| **Al** | **Mg** | **Si** | **Cu** | **Fe** | **Mn** | **Cr** | **Zn** | **Ti** |
|---|---|---|---|---|---|---|---|---|
| Bal. | 0.3-0.7 | 0.61 | ≤0.2 | ≤0.5 | 0.08 | 0.018 | 0.004 | 0.018 |

Table 1.4: Chemical composition of the 6016 aluminium alloy T4 (% wt)

The 6xxx series aluminum alloys mainly contain Mg and Si, due to their superior strength to that of the $Mg_2Si$ precipitation strengthening during aging [37]. Addition of a small amount of Cu improves the precipitation kinetics, while this shows the poor corrosion resistance [32], [52]. Zr and Ti additions decrease the grain sizes, which affects the recrystallization during the rolling and extrusion [56]. It was reported that increasing Si content, decreasing Mg/Si ratio and adding 0.3 wt% Cu were generally used to improve the tensile ductility and formability of the 6xxx aluminum alloys [44], [57]. Typical characteristics of 6xxx series alloys are:

- High hot formability: they are considered the best alloys for extrusion;
- Good cold deformability, both in the annealed state and in the T4 condition (solubilization and natural aging);
- Good corrosion resistance
- Good weldability
- Excellent mechanical strength, as function of the amount of alloying elements, in the T6 condition (solubilization and artificial aging).

The mechanical properties of 6xxx alloys are reported in the table 1.5 [31].

| | |
|---|---|
| Ultimate tensile strength, $R_m$ | 250÷350 MPa |
| Yielding stress, $R_{p0.2}$ | 200÷250 MPa |
| Hardness | 80÷100 HB |
| Young's modulus, E | 70.000 MPa |
| Percent elongation before break | 10÷15% |

Table 1.5: Mechanical properties of 6xxx series Aluminum Alloy

## 1.3 Aluminium properties of interest for laser welding

This section will describe the most important properties influencing the welding process. The properties will be described in the order in which they appear when heating an aluminium workpiece with a laser beam. All the information in this section comes from the Doctoral Thesis *Laser Welding of Aluminium Alloys, T. Forsman* [16].

### 1.3.1 Absorption

Aluminium is highly reflective to incoming light compared to other metals as shown in figure 1.11. The absorption for light incident on a metal surface can be calculated from the optical constants called the refractive index and the extinction coefficient by the equation 1.1

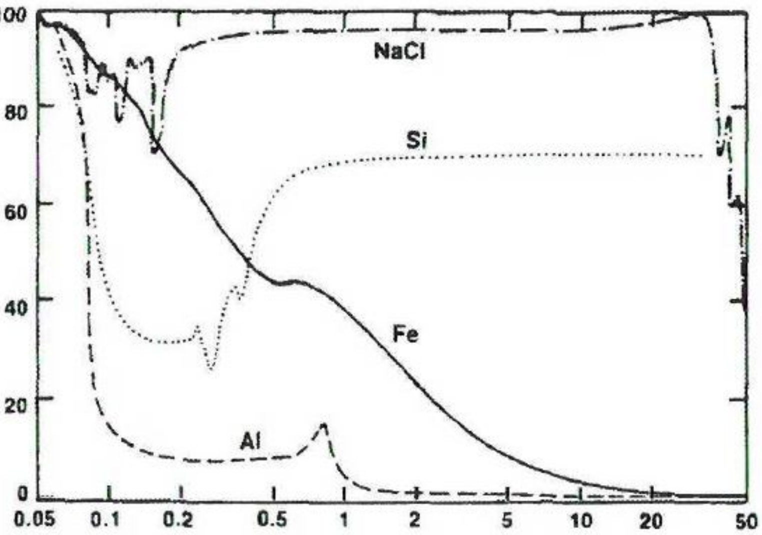


Figure 1.11: Absorptivity as a function of wavelength for NaCl, silicon, iron and aluminum

$$A = \frac{1}{2}\left[\frac{4n\cos\theta}{(n^2+k^2)\cos^2\theta+2n\cos\theta+1}+\frac{4n\cos\theta}{n^2+k^2+2n\cos\theta+\cos^2\theta}\right] \tag{1.1}$$

where:

- A = absorption
- n = refractive index
- $\theta$ = angle of incidence from normal [°]
- k = extinction coefficient

and the absorptivity (at normal incidence) is:

$$A_0 = \frac{4n}{(n+1)^2 + k^2} \tag{1.2}$$

The absorption is a function of the incidence angle of the light, the temperature of the workpiece, the surface condition and the wavelength of the light as shown in figures 1.12 and 1.13.

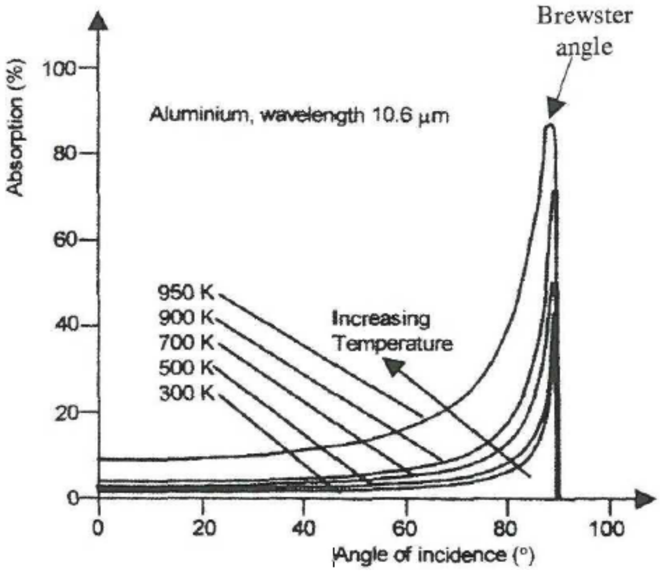


Figure 1.12: Absorption of $CO_2$ light in aluminium as a function of temperature and angle of incidence

The important parameters which influence absorption can be summarised as follows:

- A reduction in wavelength generally yields higher absorption because the photons are more energetic and therefore can be absorbed by more electrons;
- Increased temperature yields higher absorption because the phonon population increases leading to more phonon/electron energy exchanges.
- The absorption also increases when changing from solid to liquid and from liquid to gas;
- Increased oxide thickness usually yields higher absorption;

- Increased surface roughness yields higher absorption because of an increased number of reflections in the undulations. If the roughness is less than the beam wavelength the surface is perceived as flat;
- Increased incidence angle from the normal yields higher absorption up to the Brewster angle after which it decreases to zero.

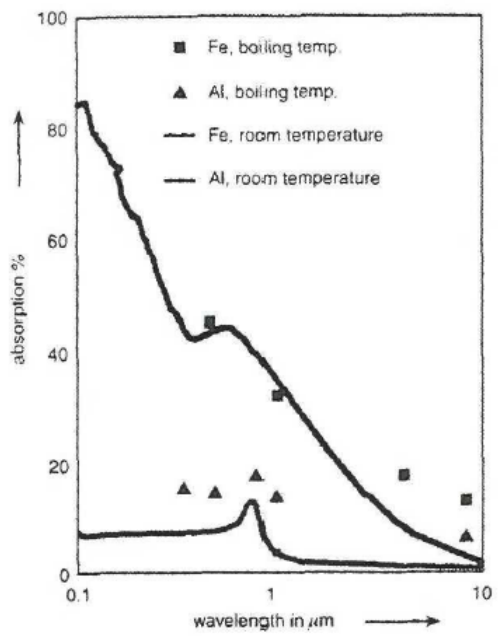


Figure 1.13: Absorption of light in aluminium and iron as a function of wavelength and temperature [16]

### 1.3.2 Thermal conductivity

The flow of heat in a medium goes from hot to cold in order to minimise the entropy according to Fourier's first law:

$$q_y = -k\frac{\partial T}{\partial y} \tag{1.3}$$

where:

- $q_y$ = heat flow in y direction [W/m$^2$],
- k = thermal conductivity [W/mK],

- y = distance [m].

The thermal conductivity of a material is a function of its structure and bonding and reflects the ease or difficulty involved in the transfer of energy through the material by elastic vibrations of the lattice and by free electrons moving through the lattice. Impurities, dislocations and second phases all restrain movement and therefore metal alloys have lower thermal conductivity than the pure metal. When a laser heats the surface of a workpiece the heat will flow hemispherically (three-dimensionally) into the material. The flow of heat into the surrounding air can be neglected since the thermal conductivity of air is only 0.024 W/mK. During keyhole welding (see laser welding chapter) the heat source changes from a surface point into something that could ideally be referred to as a vertical line source from which heat flows laterally (two-dimensionally). This is the way in which laser welding was traditionally modelled. If a vertical line source is applicable the thermal conductivity will not greatly influence the weld width. Convection (heat flow by liquid movement in the weld melt) caused by temperature differences acts as an extra heat transfer mechanism at the top surface and, in the case of a through weld, also at the bottom surface of the sheet [16].

### 1.3.3 Melting and boiling point

The melting point of aluminium is low compared to other metals at 660 °C. Alloying can decrease the melting point but usually by no more than ten degrees. *T. Forsman* has shown that the low melting point is the principal reason for the widening of the weld as shown in figure 1.14. Considering the relatively high boiling point of 2470 °C aluminium has a large molten temperature range. This large molten range means that aluminium melt pools are broader and more extensive than those of other metals [16].

### 1.3.4 Viscosity of melt

The viscosity of pure aluminium melt is relatively low compared to other metals. At 850 °C the viscosity of aluminium is for instance similar to that of water at room temperature. With the additions of alloying elements and the presence of surface oxides it

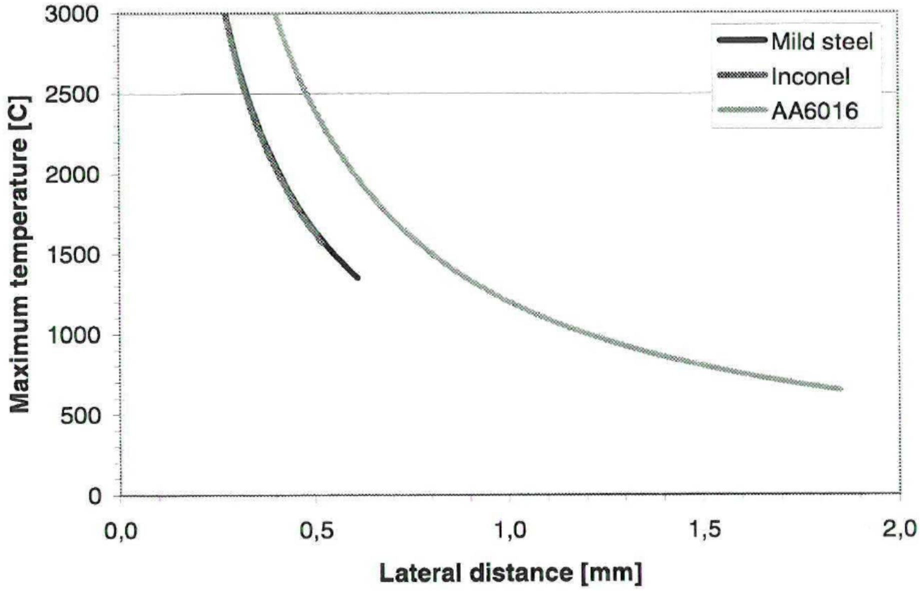


Figure 1.14: Peak temperature as a function of radial distance in three metals with varying properties

is however likely that the viscosity increases slightly when aluminium alloys are being welded. The viscosity of the melt strongly influences its stability during welding. In addition the low viscosity of aluminium increases the risk of the melt sagging or an incompletely filled groove at full penetration welding [16].

### 1.3.5 Surface tension of melt

The surface tension of aluminium melt is roughly half that of iron at their respective melting points. It is however complicated to predict the surface tension of the alloys because some alloying elements influence the surface tension strongly even at low concentrations. The surface tension of metals decreases with increased temperature. During welding this has the effect that the melt which is hottest, close to the laser heat source, is forced to the sides of the melt pool, leading to stirring. This stirring, named after Marangoni, takes place as long as the laser is heating up more melt. Marangoni stirring increases the heat transfer by convection at the surface during welding leading to widening of the weld.

## 1.4 Laser Welding

Nowadays, the main welding process used for the realization of the TWBs is the laser welding. A laser is a high-power density heat source. Therefore, 'laser welding' is recognized as an advanced process to join materials with a laser beam of high-power, high-energy density. A laser consists of a gas or crystal medium stimulated by an energy source which emits radiation of one wavelength which is also in phase. By the use of mirrors, part of the emitted light is reflected back into the medium creating an amplifying effect. Today there are hundreds of types of commercial lasers but only $CO_2$, Nd:YAG, Excimer and diode lasers are available at powers high enough to be used for material processing purposes [16]. In the figure 1.15 it's reported a comparison of the power density profiles for different welding process.

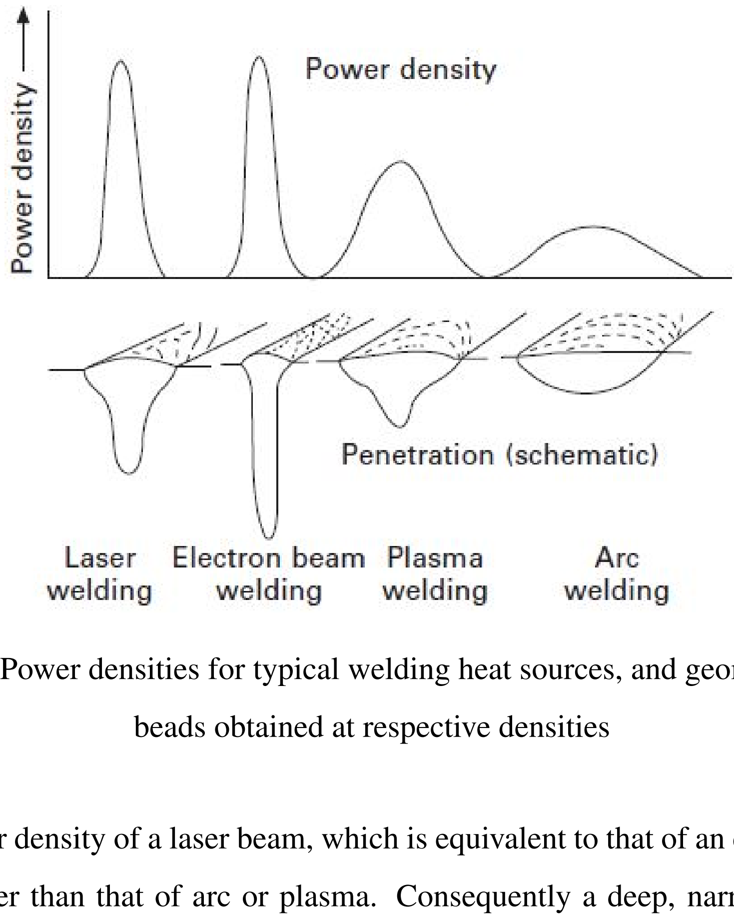


Figure 1.15: Power densities for typical welding heat sources, and geometry of weld beads obtained at respective densities

The power density of a laser beam, which is equivalent to that of an electron beam, is much higher than that of arc or plasma. Consequently a deep, narrow keyhole is formed during welding with a high-power-density beam of laser or electron, and a deep, narrow penetration weld can be effectively produced [24]. Moreover, the speed travelling of the laser welding can be much higher than those of plasma and arc welding. Among all the welding processes, laser welding can produce a variety of joints of metals or plastics ranging from very thin sheets of about 0.01 mm thickness to thick plates of about 50 mm in the shielding gas such as helium (He), argon (Ar) or sometimes nitrogen ($N_2$) under the air environment, and has gained great popularity as a promising joining technology with high quality, high precision, high performance, high speed, good flexibility and low distortion [41] - [43]. To control the formation of welds for a good weld quality the combination of the output power, welding speed, focal position, shielding gas and position accuracy should be correctly selected [14]. Schematic representation of laser welding is shown in figure 1.16.

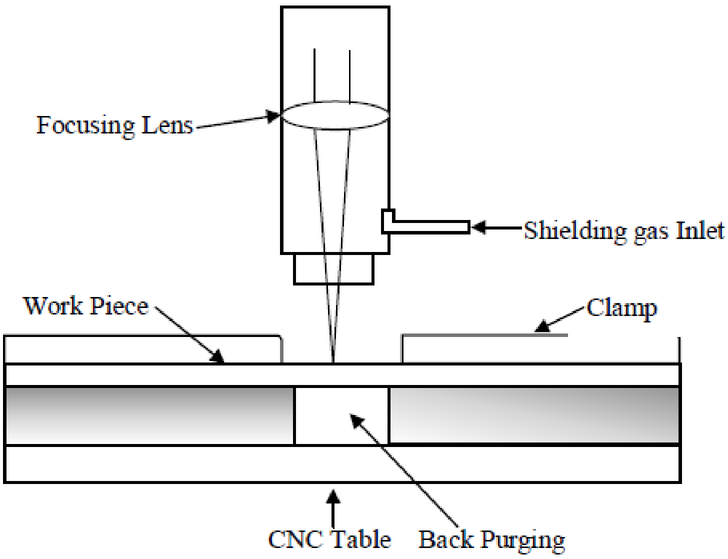


Figure 1.16: Schematic Representation of laser welding

The effectiveness of laser welding depends greatly on the physical properties of the material to be welded like absorptivity of laser beams, thermal conductivity, coefficient of thermal expansion, melting and boiling temperatures, wide solidification constituents and surface tension effect. Shorter wavelength Nd-YAG Laser has high absorptivity and thus less power is required with the Nd-YAG laser than CO2. At the same output power, smaller spot size means higher power density but the welds may become narrower than necessary or even not fully fused. Laser welding seams are usually less than one quarter of the width of a tungsten-arc inert gas weld (TIG) for the same material thickness. Joint fit-up and beam alignment are more critical for a small spot size as small spot size may also lead to more loss of elements by vaporization causing undercut and under fill defects due to high power density. Thus small spot size cannot ensure good welding performance for Nd: YAG laser beam.

Important aspects to consider during a laser welding process are that:

- The position of focal points has an important influence on welding process and quality. The focal plane should be set where the maximum penetration depths or best process tolerances are produced. Focal position on the work piece surface produces smallest weld width while any deviation (above or below the surface) leads to wider welds;

- The penetration depth and weld width both decrease linearly with increasing welding speed in general. Decrease in welding speed will lead to little increase in penetration depth but in turn will increase weld width and Heat affected zone (HAZ). Too high welding speed can increases the brittleness of the fusion zone in selected materials;

- The surface condition of material influence the energy absorption of incident laser beam as well as the threshold power density for keyhole welding. Nearly 100% absorptivity can be obtained after the formation of keyholes due to reflections in the keyhole.

During the course of this research a Nd:YAG Laser was used. A solid Nd:YAG laser beam is typically one of two types (continuous and impulse) defined according to the means of transferring energy. The impulse laser beam used herein, outperforms the continuous one for application in welding small components, because of its lower required initial power and precise positioning. Figure 1.17 depict the confguration of the Nd:YAG laser beam welding device.

As shown, the laser is generated, guided, and focused through an optical lens to constrain within 0:60 ± 0:02 mm and then projected onto the workpiece through the fibre optics with focal length 60 mm. Furthermore, the workpiece can be made to pass

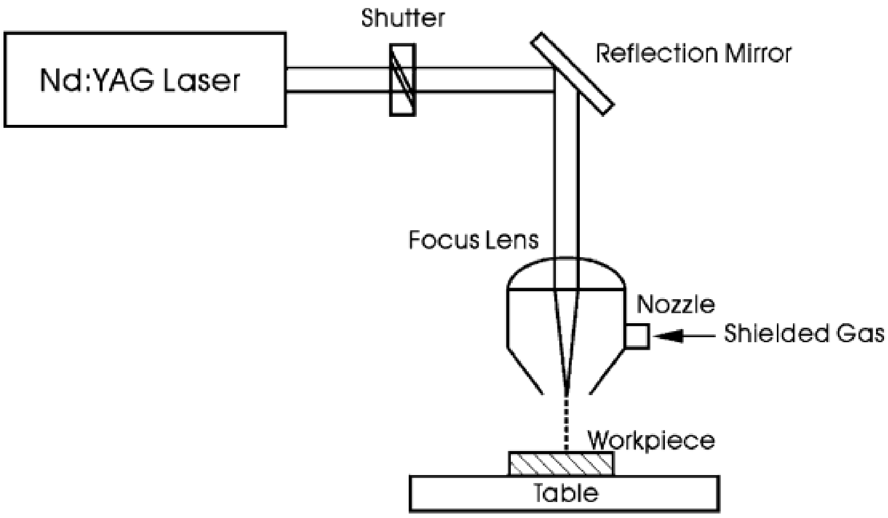


Figure 1.17: The Nd:YAG laser welding system, the workpiece is conveyedthrough a CNC holding device

through a computerized numerical control (CNC) holding device for precise positioning [35].

Two different laser welding techniques can be applied:

- *Conduction Mode Laser Welding*

  This welding technique offers less perturbation to the system because the laser radiation does not penetrate to the material being welded and the surface of the material remains unbroken. As a result the conduction welds are less susceptible to gas entrapment during welding. As mentioned above conduction welding is less efficient as it faces a primary loss of energy by reflection. Once energy is absorbed, surface is melted and the depth of melting is limited by the conduction of the energy to the subsurface and hence called conduction limited welding (fig.1.18a).

- *Key Hole Laser Welding*

  In deep penetration or keyhole welding (fig.1.18b), there is sufficient energy/unit length to cause evaporation and hence, a hole forms in the melt pool. The 'keyhole' behaves like an optical black body as when the radiation enters the hole, it is subjected to multiple reflections before being able to escape. The hole is traversed along the joint with the molten metal ahead of the keyhole flow along the sides of the keyhole and solidifying at the back. To perform keyhole welding, a laser beam having a power density >106 W/cm$^2$ is focused on the surface of the metal work piece. The transition from conduction mode to deep penetration mode occurs with the increase in laser intensity and duration of laser pulse applied to the work piece [14].

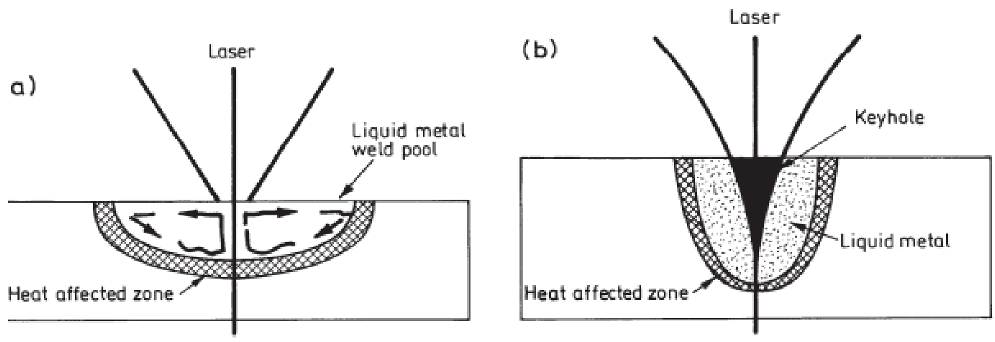


Figure 1.18: (a) Conduction melt pool (semi-circular) (b) deep-penetration (key hole) welding

Finally, it is interesting to note the advantages and disadvantages of the laser welding process.

*Advantages of Laser Welding*

- Joining of widely dissimilar materials is possible
- Reduced post weld reworks
- High processing speed
- Welds at atmospheric pressure
- Easy to automate
- Good quality : narrow and deep weld seam
- No mechanical contact between the laser equipment and the work pieces

- Low but concentrated heat input, which results in low and predictable distortion levels

*Disadvantages of Laser Welding*

- High cost of equipment and maintenance
- High reflective materials are difficult to weld
- Poor gap bridging ability, which leads to high requirements on joint preparation
- Loss of volatile elements

### 1.4.1 Laser Welding of Aluminium alloys

In spite of the above advantages of laser welding, and in spite of the fact that it is quite widely used nowadays, its application on aluminum alloys needs further development and improvement. The reason lies in the physical properties of these alloys, including their high thermal conductivity and high reflectivity. In fact, aluminium is usually described as being very reflective to laser radiation. Typical absorption figures are presented in table 1.6.

| Absorption of Nd:YAG light (1.06 $\mu$m) | Comment |
|---|---|
| 11% | Calculated |
| 5% | Experimental |
| 11% | Experimental |
| 9% | Calculated |
| 12% | Experimental |

Table 1.6: Absorption in aluminium; data from the literature [16]

This type of absorption measurement usually shows how low intensity radiation at normal incidence is absorbed on a flat aluminium surface at room temperature. The absorption has however been found to depend on the wavelength of the incident light, the angle of incidence to the surface, the surface temperature and the surface roughness. This makes it difficult to compare results and consequently they often differ [16]. Another limitation concerns the thermal conductivity. The thermal conductivity coefficient of aluminum alloys depends on several factors, such as temperature, the amount of alloying elements (see figure 1.19) and the heat treatment applied to the alloy.

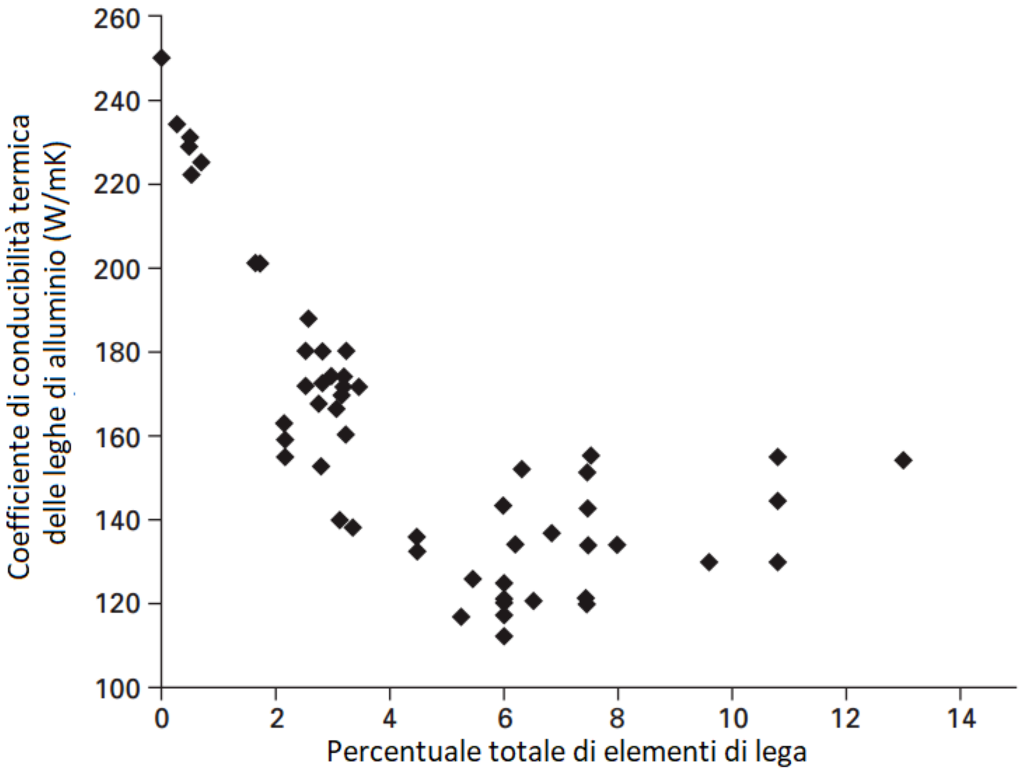


Figure 1.19: Thermal conductivity of some aluminum alloys at room temperature as a function room temperature as a function of the total percentage of alloying elements

The relatively high value of thermal conductivity causes rapid heat transfer when the alloy is subjected to a laser beam. This is a major disadvantage because the heat diffuses throughout the part, hindering a concentration of energy in the melt pool. As a result, aluminum alloys require higher laser beam energies than other alloys to be welded.

# Chapter 2

# Aluminum Tailor Blanks

The first TWBs were produced by seam welding employing steel, while nowadays the production is realized by means of laser welding using both steel and aluminium alloy: the use of materials with low density or high strength leads to a weight reduction and that's the reason why their use it is increasingly gaining interest both by the automotive and aerospace industries [34, 38]. For example, both the 5xxx and 6xxx series aluminum alloys are typically supplied to automotive manufacturers, where they are used for car body parts and door structural components. This is because of their unique properties, including moderate strength, high corrosion resistance, weldability, and easy forming characteristics [48, 53].

However, the application of aluminium or high strength steels for the body in white is limited through the low formability [21]. Another aspect limiting the use of aluminium TWBs is the laser welding which, although it has many advantages and its use in automated industries is constantly growing, remains a process to be developed and improved: the main reason for this is likely to be the high investment costs involved for small companies. It is important to remember that the more a laser works the more economical it gets and for purposes where high precision and flexibility is needed there is no welding process to match it. In cases where thin aluminium alloys are to be joined at high speed, laser welding technology is expected to dominate [16].

## 2.1 State Of Art

During the years, different studies have been carried out to consolidate the use of steel TWBs, however, there are few studies concerning aluminium alloys tailor blanks.

*Friedman e Kridli (2000)* [17] investigated on the mechanical and microstructural properties of laser-welded joints between 5xxx and 6xxx series aluminum alloys. The results of tensile tests showed that in joints between sheets of the same thickness the breakage occurred in welding, while in joints between sheets of different thicknesses the breakage occurred in the base metal of lower thickness. The cause of this behavior has been identified in the geometry of the welding seam, because in the case of different thicknesses there is sufficient material to create a transition zone between the two dimensions while in the case of equal thicknesses a reduction of the resistant section at the seam is more likely to occur. It has also emerged that the smaller thickness sheet has undergone a much greater deformation at breakage than the larger thickness sheet. Finally, tests were conducted on formability (limiting dome height tests) which showed that this property depends on the orientation of the welding line: Good results were observed with the welding line inclined by 45°, compared to the stretch direction of the sheet.

A study by *Shakeri et. al (2002)* [45] provided for the carrying out of formability tests (limiting dome height) on Nd:YAG laser and electronically beam joints between aluminium sheets EN AW 5754 with different thickness ratios. Two fracture modes have been observed: in the welding seam and in the base material. The position of the fracture seems to depend on several factors, including the thickness ratio, the orientation of the weld and the presence/absence of surface defects. With the same other parameters, it has emerged that the formability of the joint decreases as the thickness ratio increases. Finally, it was highlighted that the characteristics of welding are strongly influenced by the presence of welding defects, their type and their distribution. The loss of formability compared to the base material is strongly influenced by the welding quality, especially for low thickness ratios.

*Shibata et al. (2003)* [47] studied the effect of laser power and welding speed on the quality of bead-on-plate welding carried out with a double beam Nd:YAG laser (twin spot beam) on aluminum sheet EN AW 5183, identifying an acceptable range of these process parameters. Tensile tests on welds between sheets with different thickness ratios showed that the breakage occurred in the base material of minor thickness only if the minimum thickness of the welding seam was greater than at least 10% of the sheet metal of minor thickness. A formability test (ball elongation test) on a weld with a thickness of 1 mm - 2 mm has obtained a deformation equal to 70% of that of the base material of greater thickness. Finally, a real component (rear door of a car) was manufactured from the molding of an aluminum alloy TWB and its stiffness was compared with the same component made of steel, obtaining equal or higher performance.

A study conducted by *Jie et al.(2007)* [22] involved the carrying out of tensile and formability tests on Nd:YAG laser welded test pieces made of aluminium EN AW 5754 of thickness 1 mm - 1,3 mm, on the basis of which a finite element model capable of predicting the formability limits of the joint has been constructed.

*Liu et al. (2016)* [30] observed the effect of the thickness ratio on the formability of Nd:YAG laser welding between aluminium sheets EN AW 6082 using a particular process, which provides for preliminary heating (solubilization) of the TWB, moulded quenching and artificial ageing. It has been observed, through hardness measurements, how the mechanical properties of the welding have been restored following the process. In addition, it has been highlighted that the separation of the welding line from its original position due to deformation is greater for greater thickness ratios. Finally, a finite element model of the process was obtained which allowed to analyze the movement of the welding line and the distribution of deformations.

*Bagheri et al. (2020)* [5] compared the tensile strength and formability of joints between aluminium sheets EN AW 6061 with thicknesses of 1.2 mm - 0.8 mm obtained by means of three different welding methods: CO2 laser, Friction Stir Welding (FSW) and Friction Stir Vibrating Welding (FSVW). The optimal parameters for each method have been identified by applying the Taguchi method, varying three parameters on three levels and maximizing the formability of welded joints measured by appropriate tests (limiting dome height tests). Using these parameters, the formability limit curves were constructed for each welding method. FSW and FSVW welds have a higher formability and strength compared to laser welds, due to the better microstructure of the weld resulting from these methods, which has smaller grain sizes.

*Bergamo S. (2021)*, during his Master's thesis research at Politecnico di Torino and supported by the company *CO.ST.AT. S.r.l.*, studied the effect of welding parameters on the mechanical properties of Aluminum Tailor Blanks made of EN AW5754 and EN AW6016 alloy, with a variable thickness of 2mm and 1.2mm. Through this study it has been confirmed that the variation of the laser power, of the welding speed and of the focal position have a great impact on the material properties. The tests carried out on the study conducted by Bergamo S. (2021) aimed to evaluate the formability and the tensile strength of the joint and the quality of the welding process, for this reason tensile tests, Erichsen cupping test and metallography have been performed. Applying the optimization techniques of the Response Surface Methodology, the welding parameters were explored by means of a three-factor Box-Behnken Design centered on the current working point $L_0$, equal for both alloys, with the aim of confirming the effectiveness of such a combination of parameters, or to identify new combinations that can improve the process, including through the approximation to the experimental data of multiple linear regression models for the two observed responses. Multiple linear regression models have been developed for the Erichsen Index response for both alloys, and combinations of alternative parameters to $L_0$ have been identified, which can improve the process, both in terms of mechanical properties obtainable, and in terms of time or cost reduction. However, the efficacy of these combinations was not verified by an appropriate experiment. No valid regression model could be obtained for the Ultimate Tensile Strength response, in fact none of the models obtained from the comparison with the experimental data was in fact adequate and sufficiently accurate for the prediction of new observations of the response.

## 2.2 Aim of the Study

As can be seen from the previous section, there are few studies in the literature regarding their application for TWB welding, particularly for aluminum alloys. Strongly believing in the potential of tailor blanks and laser welding, the aim of this research is to contribute to the development of this innovative technique, of strong interest to the automotive sector, but also aeronautics. Therefore, we want to understand the effect that welding parameters have on aluminum alloy sheets of different thicknesses by investigating the microstructure and mechanical properties of the joint. The current study will be the continue and the deepening of the one carried out by *Bergamo S.*, in fact it has been conducted at Politecnico di Torino, and it has been supported by the same company *CO.ST.AT. S.r.l.*. Although he has obtained good results, a validation of the same is necessary. As mentioned earlier, *Bergamo S.*, by means of a statistical analysis, has obtained a set of optimal parameters for the laser welding process on aluminum alloys. The aim is to highlight the criticalities encountered, both in the laser welding process and in the experimental tests, making changes to the equipment already used. So, starting from the optimal sets of welding parameters, an experimental campaign was carried out using Taguchi methods for the EN AW5754 and EN AW6016 alloys. In order to characterize the quality of the welded joint, tensile tests, Erichsen cupping tests and metallographic analysis have been performed.

It is important to know that the process parameters used are divided by a value $x$, since this is sensitive data of the company *CO.ST.AT. S.r.l.*

# Chapter 3

# Experimental Procedure

## 3.1 Design of experiment (DOE)

The technique of defining and investigating all possible conditions in an experiment involving multiple factors is known as the design of experiments (DOE). In the literature, this technique is also referred to as factorial design. Design of experiments concepts have been in use since Sir Ronald A. Fisher's work in agricultural experimentation during the late 1920s. Numerous applications of this approach, especially in the chemical and pharmaceutical industries, are cited in the literature. [40]. In order to perform a DOE it is necessary to define the problem and choose the variables, which are called *factors* or parameters by the experimental designer. A design space, or *region of interest*, must be defined, that is, a range of variability must be set for each variable. The number of values the variables can assume in DOE is restricted and generally small. At first there is no knowledge on the solution space, and it may happen that the region of interest excludes the optimum design. If this is compatible with design requirements, the region of interest can be adjusted later on, as soon as the wrongness of the choice is perceived. The DOE technique and the number of levels are to be selected according to the number of experiments which can be afforded. The term *levels* refers to the number of different values a variable can assume according to its discretization. The number of levels usually is the same for all variables, however some DOE techniques allow the differentiation of the number of levels for each variable. In experimental design, the objective function and the set of the experiments to be performed are called *response variable* and *sample space* respectively [13]. A lot of DOE techniques are present and used. A full list of these techniques would go beyond the scope of this study, for this reason only the one of our interest will be presented.

### 3.1.1 Introduction to the Taguchi method

The Taguchi method was developed by Genichi Taguchi in Japan to improve the implementation of off-line total quality control. The method is related to finding the best values of the controllable factors to make the problem less sensitive to the variations in uncontrollable factors. This kind of problem was called by Taguchi *robust parameter design problem*. Taguchi method is based on mixed levels, highly fractional factorial designs, and other orthogonal designs. It distinguishes between *control variables*, which are the factors that can be controlled, and *noise variables*, which are the factors that cannot be controlled except during experiments in the lab. Two different orthogonal designs are chosen for the two sets of parameters. We call *inner array* the design chosen for the controllable variables, and *outer array* the design chosen for the noise variables. The combination of the inner and the outer arrays give the *crossed array* which is the list of all the samples scheduled by the Taguchi method. Combination means that for each sample in the inner array the full set of experiments of the outer array is performed. A Taguchi design is a designed experiment that lets you choose a product or process that functions more consistently in the operating environment. Taguchi designs recognize that not all factors that cause variability can be controlled. These uncontrollable factors are called noise factors. Taguchi designs try to identify controllable factors (control factors) that minimize the effect of the noise factors. During experimentation, you manipulate noise factors to force variability to occur and then determine optimal control factor settings that make the process or product robust, or resistant to variation from the noise factors. A process designed with this goal will produce more consistent output. A product designed with this goal will deliver more consistent performance regardless of the environment in which it is used. Taguchi designs use orthogonal arrays, which estimate the effects of factors on the response mean and variation. An orthogonal array means the design is balanced so that factor levels are weighted equally. Because of this, each factor can be assessed independently of all the other factors, so the effect of one factor does not affect the estimation of a different factor. This can reduce the time and cost associated with the experiment when fractionated designs are used. Orthogonal array designs concentrate primarily on main effects. In Taguchi designs, noise factors are factors that cause variability in the performance of a system or product, but cannot be controlled during production or product use. A signal factor is a factor, with a range of settings, that is controlled by the user during use. A signal factor is present in a dynamic Taguchi design, but is not present in a static Taguchi design. In a dynamic response design, the quality characteristic operates along a range of values and the goal is to improve the relationship between a signal factor and an output response. In a static response design, the quality characteristic of interest has a fixed level.

### 3.1.2 Design of the Taguchi Experiment

In our case a static Taguchi Design has been chosen. First of all control factors for the inner array and noise factors for the outer array must be chosen: in our case the control factors will be the Laser Power (W), the welding pass speed (m/min) and the focal lenght (mm). Since in this case a control of a noise factor would be too difficult and would require a very deep investigation, it will be neglected. As already said three factors will be considered, Power, Speed and focal length and they will be varied in three levels (1, 2, 3): the level 1 corresponds to the minimum value of the parameter, while the level 3 to the maximum value. Two response will be analyzed separately: the Ultimate tensile strength (MPa) and the Erichsen Index (mm). A total amount of 9 runs will be performed, obtaining an L9 ($3^3$) orthogonal array design. On the notation the number close to L indicates the number of runs, the first number under rackets indicates the number of levels for each factor, and the exponent indicates the number of factors.

| Run | Control factors and levels | | |
| --- | --- | --- | --- |
| | Power (W) | Speed (m/min) | Focal length (mm) |
| 1 | 1 | 1 | 1 |
| 2 | 1 | 2 | 2 |
| 3 | 1 | 3 | 3 |
| 4 | 2 | 1 | 2 |
| 5 | 2 | 2 | 3 |
| 6 | 2 | 3 | 1 |
| 7 | 3 | 1 | 3 |
| 8 | 3 | 2 | 1 |
| 9 | 3 | 3 | 2 |

Table 3.1: Taguchi L9 orthogonal array

In the table 3.2 the levels of the welding parameters are shown. The value of the middle level has been chosen according to the results achieved by Bergamo S. (2021) and the range of variation has been dictated by the experience of the welder. All the values of Power, speed and focal length are divided by a coefficient $x$ because sensitive company data. As already said, in this study, differently to the one conducted by

| Level | Power (W) | Speed (m/min) | Focal length (mm) |
| --- | --- | --- | --- |
| 1 | 228 | 0.24 | 0.16 |
| 2 | 260 | 0.32 | 0.24 |
| 3 | 292 | 0.40 | 0.32 |

Table 3.2: Laser welding parameters used with the 5754 Alloy (All the parameters are divided by a coefficient $x$)

Bergamo S. (2021) the use of the Helium as shielding gas was not possible, and this lead to a difficulty in obtaining a proper weld joint on the 6016 alloy sheets. It is known from the literature that macrostructure of the welded joint also depends on the shielding gas used and its flow rate as it affects the molten pool, plasma generation and plasma plume behaviour [14]. So, for what concerning the 6016 alloy, an increase in the power was necessary to obtain a satisfactory result. The laser welding parameters used for the 6016 alloy, are reported in the table 3.3. The data will be analyzed

| Level | Power (W) | Speed (m/min) | Focal length (mm) |
|---|---|---|---|
| 1 | 368 | 0.24 | 0.16 |
| 2 | 400 | 0.32 | 0.24 |
| 3 | 432 | 0.40 | 0.32 |

Table 3.3: Laser welding parameters used with 6016 Alloy (All the parameters are divided by a coefficient $x$)

using the statistical software called Minitab. First of all an analysis of the means will be conducted: the mean is the average response for each combination of control factor levels in a static Taguchi design. Depending on the response, the goal is to determine factor levels that either minimize or maximize the mean. In our case, the goal will be to maximize the tensile load and the Erichsen Index (mm). Then, the standard deviation of responses will be observed. Minitab will calculates a separate standard deviation for each combination of control factors in the design.

For a deeper analysis of the data it is useful to consider the *Heat Input*: it is the amount of energy supplied per unit length of the welded workpiece and is measured in *J/mm*. The Heat Input can be computed as the ratio between the Laser Power (W) and the welding speed (mm/s), as follow in the equation 3.1:

$$HI = \frac{P}{v} \tag{3.1}$$

## 3.2 Welding process and specimens production

To obtain the specimens, at first 36 couples of aluminum sheets (122x408 mm) with two different thickness (2 mm and 1.2 mm) have been produced for each alloy and for each series of welding parameters, obtaining 18 couples of sheets for each alloy. Then sheets of the same alloy, with different thickness, have been joined together by mean of a laser butt weld along the longitudinal direction using a *TruLaser Cell Series 7040 laser system* (fig. 3.1 ,from the TRUMPF website) The laser used is a TRUMPF


Figure 3.1: TruLaser Cell Series 7040 laser system

Trudisk-4001 disc laser, with a maximum power of 4000 W and a beam wavelength of 1,030 $\mu$m. To omit the role of anisotropy on the formability behavior of TWBs, the parent specimens (to produce TWBs) were cut from the same sheet and along the rolling direction. Additionally, for all the studied TWBs, the weld line was parallel to the rolling direction. Every welding have been performed with an angle of the laser head of $\alpha = 20°$, in figure 3.2 a schematic representation of the welding process is depicted. In order to keep close the two sheets during the welding procedure, a fixing system has been designed and produced by *Bergamo S. (2021)*. Following the comments of *Bergamo S.*, and observing the deformation of the fixing system due to the heat, it was necessary to apply some modification to the fixing system: the fixing plates have been enlarged, by increasing both width and thickness, aiming to improve

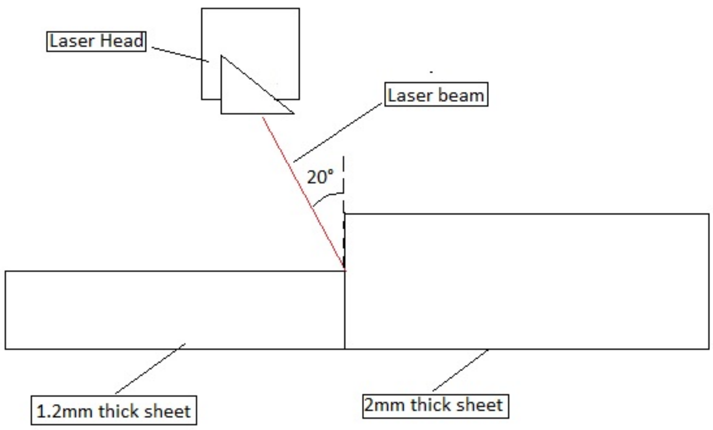


Figure 3.2: Scheme of the laser welding process

their robustness. Besides, a chamfer was created in the inner part of both the fixing plates, as to guarantee the passage of the laser beam with different inclination angles. The final result of the fixing device is depicted in the figure 3.3. Before the welding

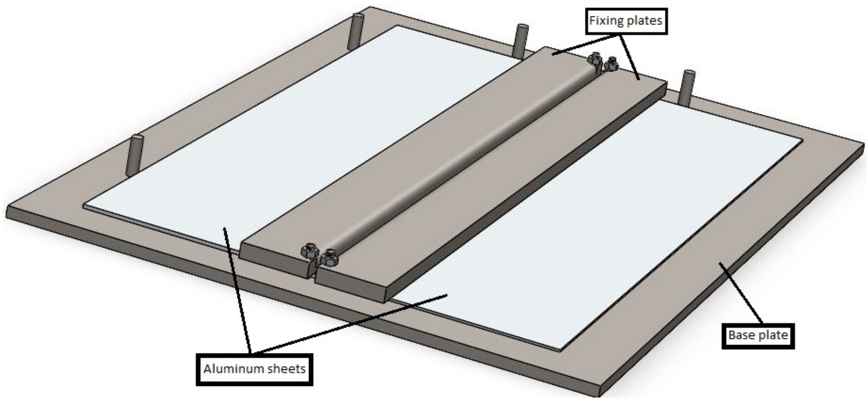


Figure 3.3: Fixing System for welding process

process, every sheet has been dampened with a a cloth soaked in acetone, then it has been scratched with an abrasive disc, in order to remove the surface oxide layer,the alumina. This preparation will help to produce a joint between the two sheets. Due to problems related to welding machine, a shielding gas hasn't been used during the welding process, unlike how Bergamo did it: during his research Helium was used as shielding gas. This aspect will be taken into account throughout the research, in fact it is know from literature that macro structure of the welded joint also depends on the shielding gas used and its flow rate as it affects the molten pool, plasma generation and plasma plume behaviour. As in laser welding of Al-alloy plasma generation is high, in order to push plasma plume out of the weld, higher shielding gas flow rate is necessary specially in case of low density gas like He (0.1664-0.1785 kg/m3) [14].

In the figure 3.4 the welding process can be appreciated.

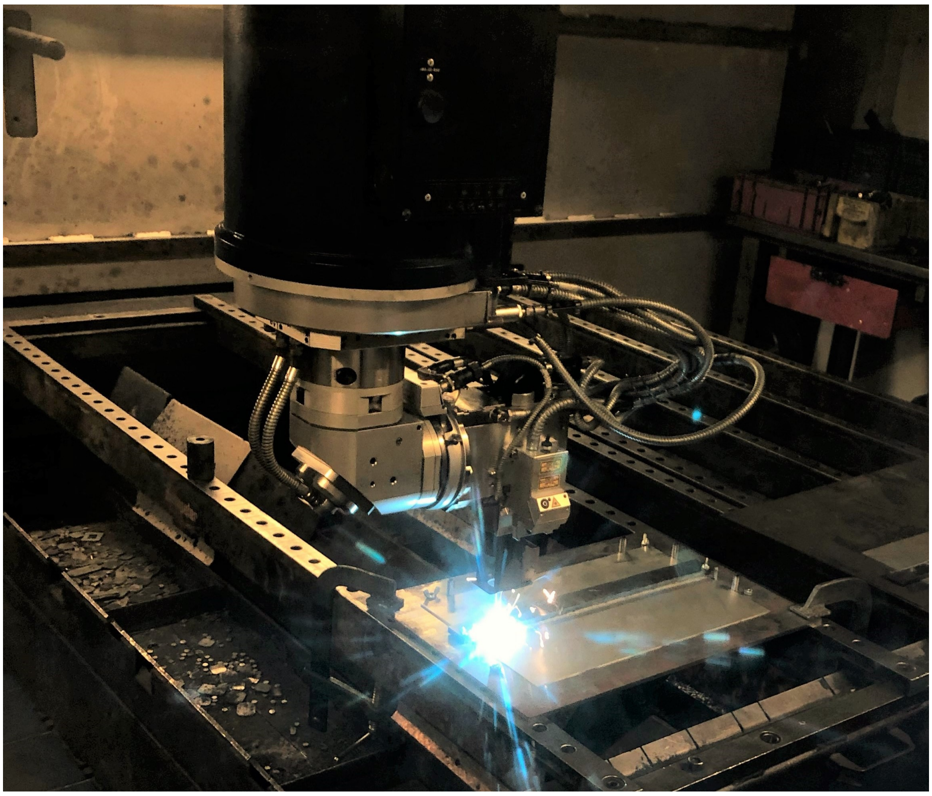

Figure 3.4: Laser welding process

Finally, the specimens have been obtained through a waterjet cutting process (fig. 3.5): this type of cutting process has been chosen as it provides an excellent surface finish and it does not produce any thermally altered areas, therefore the microstructure of the material is not altered [15], in accordance with the requirements of the *UNI EN ISO 4136:2012 Standard (Destructive tests on welds in metallic materials — Transverse tensile test)* concerning the tensile test on welded joints [4]. The following specimens have been obtained: three circular specimens with a diameter of 90 mm for the Erichsen cupping test as prescribed by the *ISO 20482:2013 standard* [3], one specimen for the metallography and three dogbones for the tensile test.

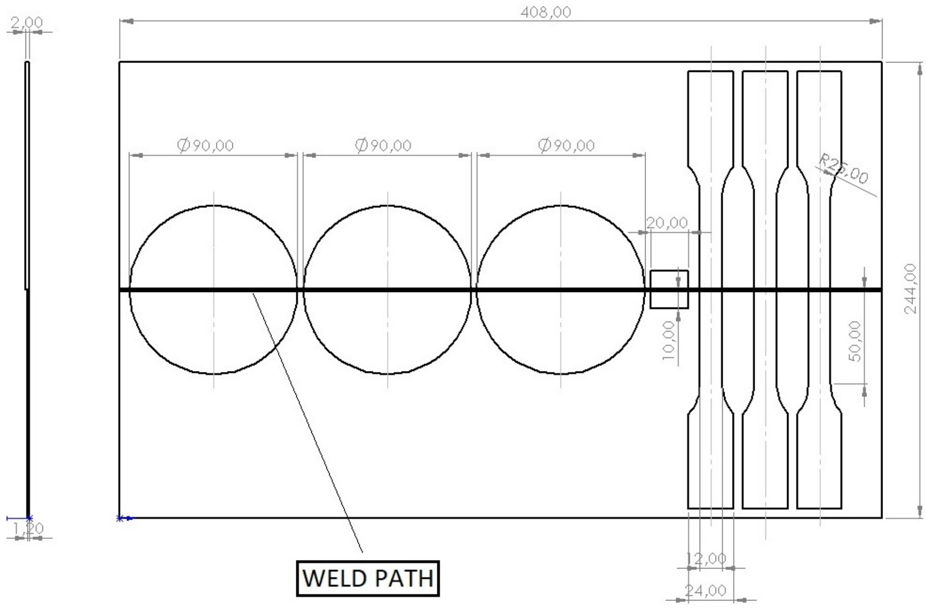


Figure 3.5: Cutted specimens

## 3.3 Tensile test

The tensile test is of fundamental importance to understand the weld performance and to check if the welded joint is as strong as the base metal. All the tensile tests have been performed in the Laboratory of *DIMEAS* of Politecnico di Torino , using a servo-hydraulic machine *Instron 8801*, and the standard *UNI EN ISO 4136:2012* has been followed. The servo-hydraulic machine is connected to the computer, where the data will be collected through a software. Once the test start the monitor of the computer will show the curve displacement-load and the test will automatically end when the machine detects the failure of the specimen. The setup of the tensile test in shown in figure 3.6 [7]. The test will output the displacement of the upper crossbar of the machine, in millimeters and the load applied, in Newton. In total, a number of 54 specimens have been tested (3 replicate for the 9 different sets of welding parameters, for each of the two alloy).

Figure 3.6: Tensile test setup

## 3.4 Erichsen cupping test

In order to properly run the Erichsen cupping, *EN ISO 20482:2013 (Metallic materials - Sheet and strip - Erichsen cupping test)* international standard has been followed, which specifies a standard test method for determining the ability of metallic sheets and strips having a thickness from 0,1 mm up to 2 mm and a width of 90 mm or greater to undergo plastic deformation in stretch forming (see fig. 3.7).

The procedure involves forming an indentation by pressing a punch, moved by a piston, with a spherical end against a test piece blocked between a die and a blank holder until the appearance of a crack. The measured depth of the indentation is the result of the test based on the movement of the punch.

Compared to a Nakazima test, in which the formability limit curves of a sheet are generated by performing indentations on several specimens with different geometry and analyzing the different states of deformation that can be obtained in the stamping operations, the Erichsen test is certainly less comprehensive in characterizing the formability of the material. However, since the aim of the study is to compare a large number of different experimental conditions in order to identify those which provide the best performance, it is more convenient to use a test easy to perform and that pro-

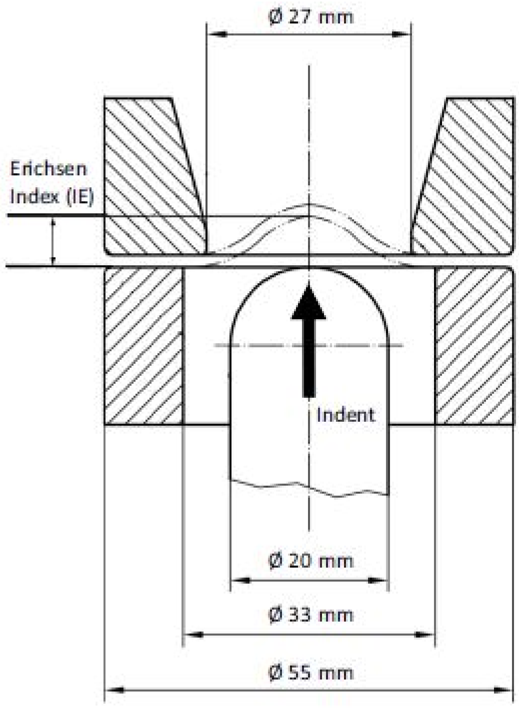


Figure 3.7: Erichsen test equipment according to the european standard (measurements in mm)

vides only one output value, clear and immediate indication of the goodness of the experimental condition observed. In addition, the Erichsen test is indicated by the *UNI EN 10359:2015 (Laser welded tailored blanks — Technical delivery conditions)* European standard, with reference to the steel TWB, as the best destructive test to check the weld quality before stamping operations [1].

### 3.4.1 Equipment Design

The *EN ISO 20482:2013* standard, in order to properly perform the Erichsen cupping test, requires the test piece to be clamped between a die and a blank holder having the geometry shown in figure 3.7.

Since the laboratories at the Polytechnic of Turin do not own a test machine suitable to perform the Erichsen cupping tests, in the studies previously conducted, a device was designed and produced. The clamping force on the test piece was applied by means of a threaded connection, while the servo-hydraulic machine Instron 8801, already used for the tensile tests, was used for the handling of the piston and the measurement of its displacement. In the designed equipment, the internal diameters and radii of the die and the blank holder have been maintained, while the external diameters have been suitably increased to allow the flange connection. The punch geometry has remained unchanged. The device has also been overturned compared to the diagram reported in the standard, because in the machine used the hydraulic actuator is located at the top. The technical drawing of the equipment is shown in figure 3.8.

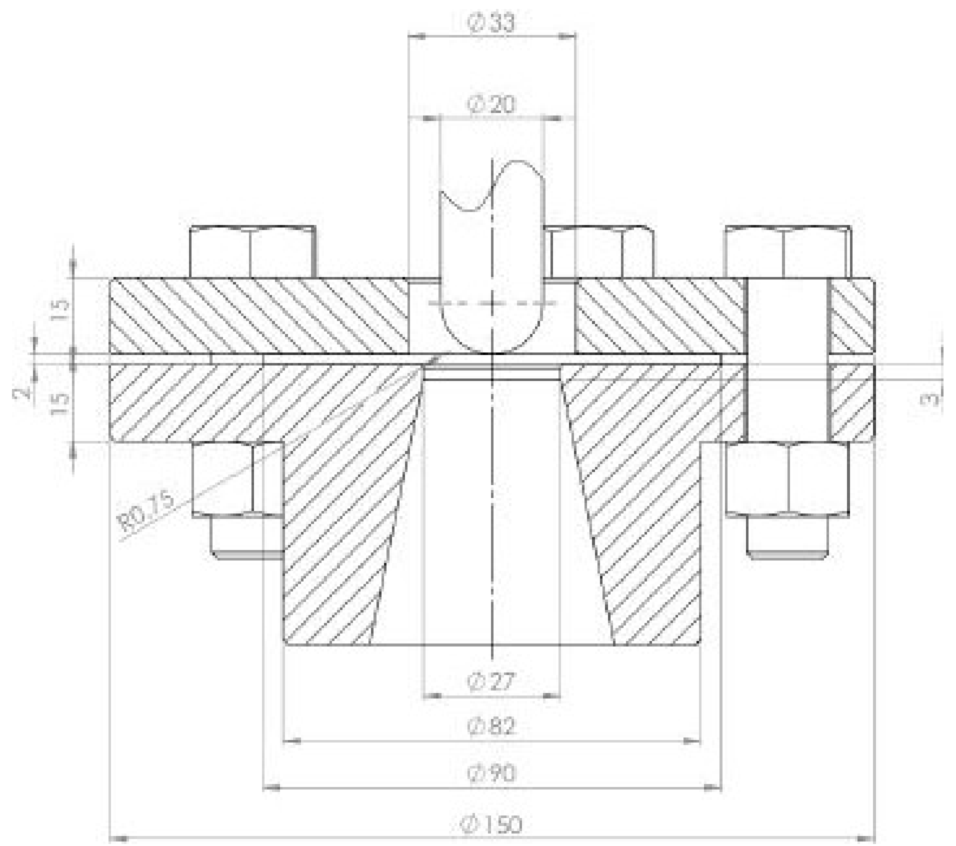


Figure 3.8: Erichsen cupping test equipment designed

All the components were modeled in 3D using Solidworks software and were manufactured by CO.ST.AT. using C40 steel. The surfaces of the die, the blank holder and the punch in contact with the specimen have been tempered to ensure the hardness required by the standard (750 HV 30). Furthermore, following the indications described in the standard, after the hardening, the punch has been polished, while the four flat surfaces of the die and blank holder have been subjected to a stoning operation, in order to obtain an adequate flatness.

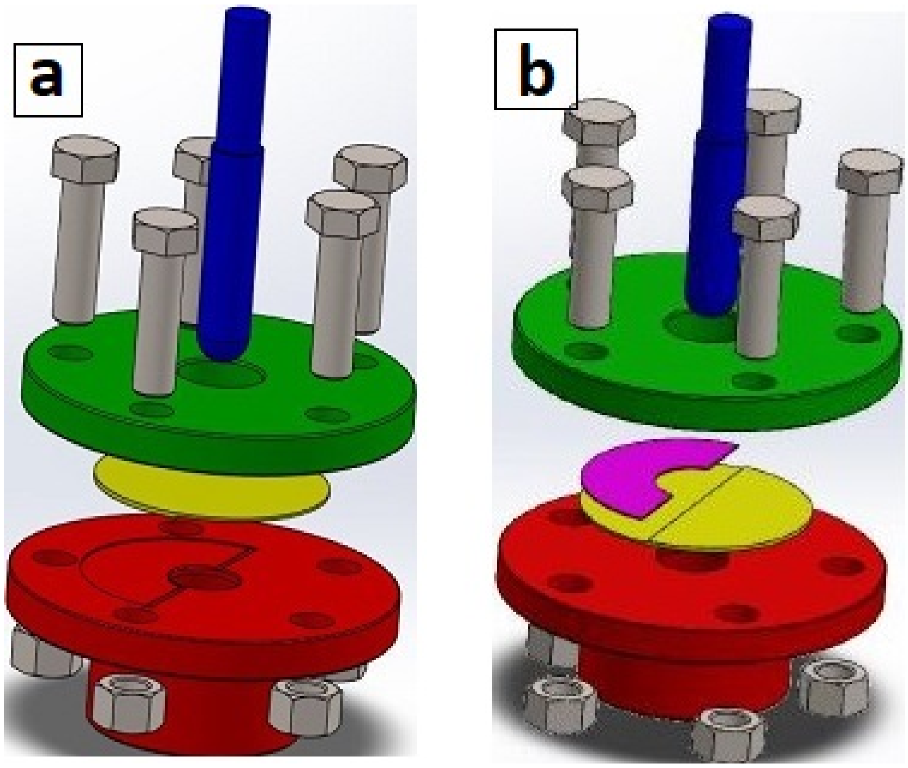


Figure 3.9: 3D model of the Erichsen cupping test equipment, the previously designed one (a) and the modified one (b)

Since the specimen have a difference in thickness (2 mm - 1,2 mm), a thickness of 0,8 mm thick steel has been produced and used to ensure uniform pressure. In the mounting position, in order that the thickness does not come into contact with the welding seam, a distance of 3 mm was provided with the interface of the two sheets. However, during the current study it was noted the difficulty in placing the thickness on the test piece and in the centering of the test piece with respect to the blank holder (see figure 3.9a). For this reason, the device has been slightly re-designed: the die has been modified creating a groove 0.8mm deep, in order to offset the difference in thickness of the test piece. Moreover a narrow groove (width 6mm, depth 0.5mm) has been created on the center of the die, so as to guarantee the preservation of the test piece seam. For the same reason, the blank holder has been modified creating the same narrow groove (see figure 3.9b).

Figure 3.10: Milling operation to modify the Erichsen cupping test equipment

The machining operations has been carried out in CO.ST.AT. using a milling machine as shown in figure 3.10 and the result is shown in figure 3.11.

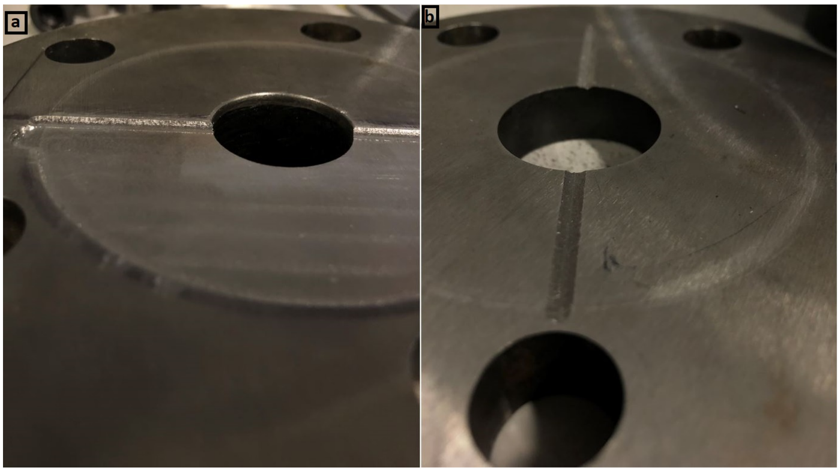


Figure 3.11: Die (a) and blank holder (b) modified

### 3.4.2 Threaded connection static verification

The tightening of the components of the device is guaranteed by 5 screws M16x60 with cylindrical head of class 8.8 burnished and oiled. The main characteristics are shown in the table 3.4.

| Measure | Code | Value | Unit of measurement |
|---|---|---|---|
| Major Diameter | $d$ | 16 | millimeter |
| Pitch Diameter | $d_2$ | 14,701 | millimeter |
| Minor Diameter | $d_3$ | 13,546 | millimeter |
| Stress diameter | $d_\mathrm{s}$ | 20,8 | millimeter |
| Thread inclination | $\alpha$ | 30 | degree |
| Head-part friction ratio | $tan\phi_\mathrm{s} = f_\mathrm{s}$ | 0,12÷0,18 | |
| Thread friction ratio | $tan\phi = f$ | 0,12÷0,18 | |
| Ultimate tensile strength | $R_\mathrm{m}$ | 800 | megapascal |
| Yielding strength | $R_{\mathrm{p0.2}}$ | 640 | megapascal |

Table 3.4: Screw Characteristics

The EN ISO 20482:2013 standard prescribes a clamping force of approximately 10 kN. Since in this research the surface on which the force is applied is greater, it was considered appropriate, for the purpose of dimensioning the threaded connection, to consider a higher clamping force, proportional to the contact surface between the blank holder and the test piece. In particular, let F be the clamping force of the test piece and S the contact surface, using the subscript 1 for this research and the subscript 2 for the case reported on the standard, has imposed itself:

$$\frac{F_1}{S_1} = \frac{F_2}{S_2} \tag{3.2}$$

From the equation 3.2 the clamping force can easily be obtained:

$$F_1 = F_2 \frac{S_1}{S_2} = 1000 \frac{(90)^2 - (33)^2}{(55)^2 - (33)^2} = 36214\,N \tag{3.3}$$

So, the force on a single screw would be:

$$F_v = \frac{F_1}{5} = 7243\ N \tag{3.4}$$

It's now possible to compute[19] the tightening torque $M_t$ as:

$$M_t = \frac{F_v}{2}\left(\frac{p}{\pi} + d_2\frac{tan\phi}{cos\alpha} + d_s tan\phi\right) = 18,72 \div 26,93\ Nm \tag{3.5}$$

To be sure that the test piece undergoes a force large enough to prevent sliding with respect the blank holder, a tightening torque $M_t$=25 Nm has been applied to the screws, using a dynamo-metric wrench. It is now necessary to calculate the axial force $F_{v,lim}$ that can be applied to the screws in a way that the screw stress limit $\sigma_{id,lim}$ is equal to the 90% of the screw yielding stress $R_{p0.2}$[19]:

$$F_{\mathrm{v,lim}} = \sigma_{\mathrm{a,lim}} \cdot A_3 = \frac{0,9R_{\mathrm{p0,2}}}{\sqrt{1+3k^2}}\frac{\pi d_3^2}{4} = 68525\ N \tag{3.6}$$

where

$$k = [\frac{2}{d_n}(\frac{p}{\pi} + d_2\frac{tan\phi}{cos\alpha})] = 0,395 \tag{3.7}$$

Now, using a design conservative approach, the lowest friction ratio has been used to compute $M_{T,lim}$:

$$M_t = \frac{F_{\mathrm{v,lim}}}{2}\left(\frac{p}{\pi} + d_2\frac{tan\phi}{cos\alpha} + d_s tan\phi\right) = 177,12\ Nm \tag{3.8}$$

Noting that

$$M_T < M_{\mathrm{T,lim}} \tag{3.9}$$

The threatened connection result statically verified.

### 3.4.3 Erichsen cupping test procedure

During the current research 54 test pieces (see fig. 3.12) have been used to properly conduct the Erichsen cupping test: 3 reruns for each set of welding parameters (9 different set of welding parameters), for the two different alloy (5754 and 6061 aluminium alloy).

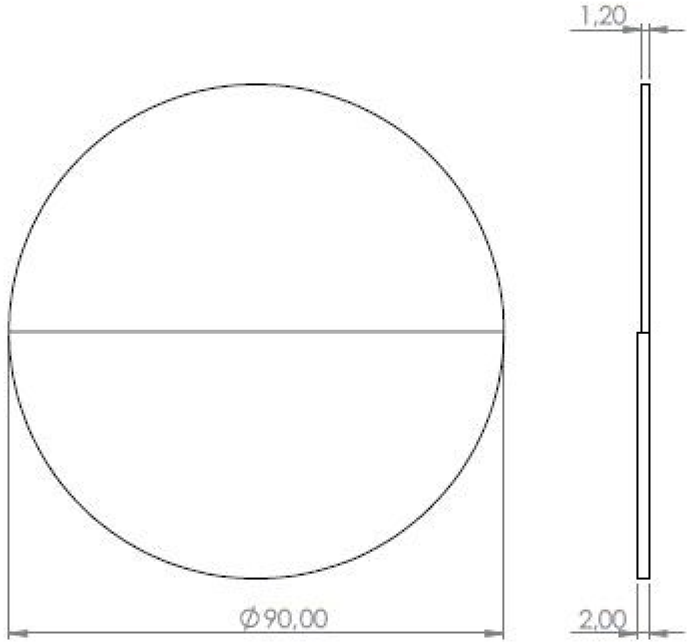


Figure 3.12: Drawing of the Erichsen cupping test specimen

The testing machine was prepared by fixing a steel platform in the lower grip and the punch in the upper grip by means of an appropriate shank (fig. 3.13). Once the test start, the displacement-load curve will be shown on the monitor of the computer. With difference with the tensile test, in this case, the servo-hydraulic machine will not recognize the failure of the specimen, so it will be taken care of by the user to stop the test once the load suddenly decreases.

It is important to reiterate that the *EN ISO 20482:2013* standard has been followed to perform the *Erichsen cupping test*. In particular the standard requires the lubrication with grease of the die and the part of the specimen in contact with the punch and the blank holder, and a moving speed of the punch of 5 mm/min (at minimum). The output data of the test will be the load (N) and the displacement of the punch, namely the *Erichsen Index (mm)*. If the test is not interrupted, the punch will continue to go down, obtaining in output a compromised *Erichsen Index (mm)*.


Figure 3.13: Erichsen cupping test setup

## 3.5 Metallographic Analysis

Metallography is performed in order to investigate on the microstructure of the metal, to understand the effect of the heat produced during the welding process and to check the quality of the joint and its defects: incomplete penetration, lack of fusion, porosity, inclusions, incorrect weld shape and size. The preparation of the microscopic analysis of the specimens includes several steps:

- Hot mounting
- Grinding and polishing

- Etching

The mounting of the specimens is fundamental for an easier handling, because of their small size. The hot mounting operation has been carried out with the press machine LECO PR-36, using bakelite, a phenolic resin. The size of the specimens is 10x10mm (see cap. 3.2). The figure 3.14 show how to place specimens on the cylinder of the press machine, which was filled with bakelite.

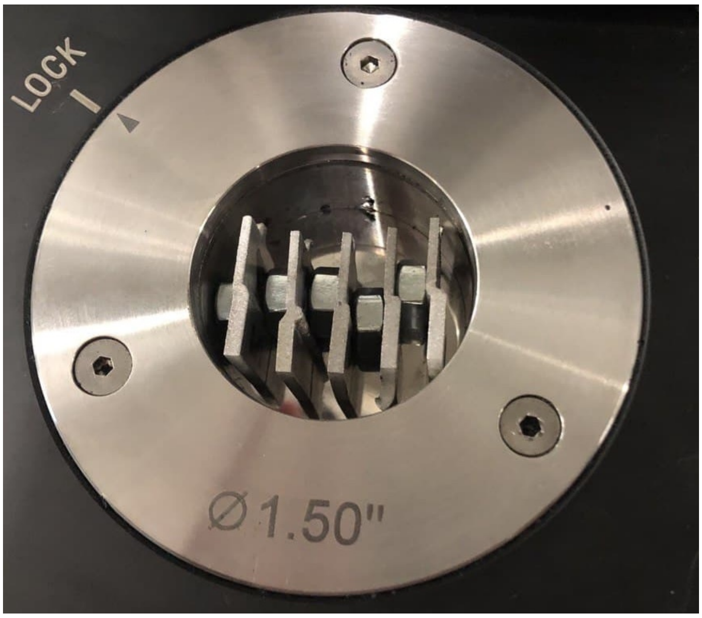


Figure 3.14: Specimens placement on the press machine cylinder

The parameters used in the hot mounting are:

- Temperature = 170 °C
- Pressure = 4100 psi
- Time = 9 minutes

At the end of the hot mounting cycle, the specimens will be like those shown in the figure 3.15. Now that specimens are easy to be handled, they need to be subjected to grinding and polishing operation, in order to obtain a smooth and glossy surface. To do so, the grinding machine *Remet LS1* has been used, with different abrasive discs of different grain sizes: 180-320-800-2500-4000 (according to the European standard,

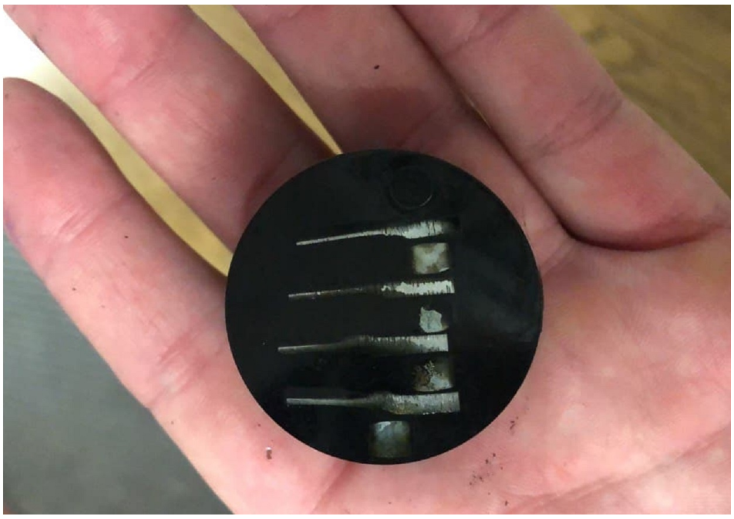

Figure 3.15: Specimens just after hot mounting

a higher number indicates a finer grain). Once a good result has been achieved, a polishing operation has been performed first using a cloth *Tecnocontrol-Polipal* with two polycrystalline diamond suspension with 3$\mu$m and 1$\mu$m particles size, then with an *Aka-Napal* cloth with colloidal silica (50 nm particles size). At the end of the polishing operations, the specimens will results as shown in figure 3.16

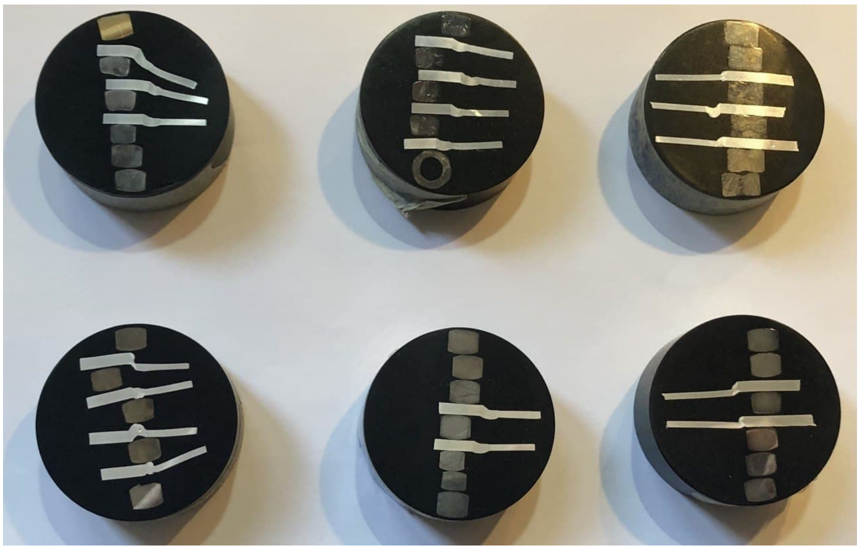

Figure 3.16: Specimens after polishing operations

Finally, a etching operation was required to ensure optimum visualization of the weld seam and the micro structure of the material. The test specimen has been put in contact with an acid solution, which corrodes in a different way regions of the material with different chemical-physical characteristics. This allows to highlight the grain edges of the material and to distinguish the grains with different orientations. This operation has been performed at DISAT laboratories of Politecnico di Torino, using a Keller's reagent with the following composition:

- 2 ml - HF 48%
- 3 ml - HCl
- 5 ml - $HN0_3$
- 190 ml - $H_2O$

So, all the specimens were observed under a optical microscope (example of an observation is in figure 3.17

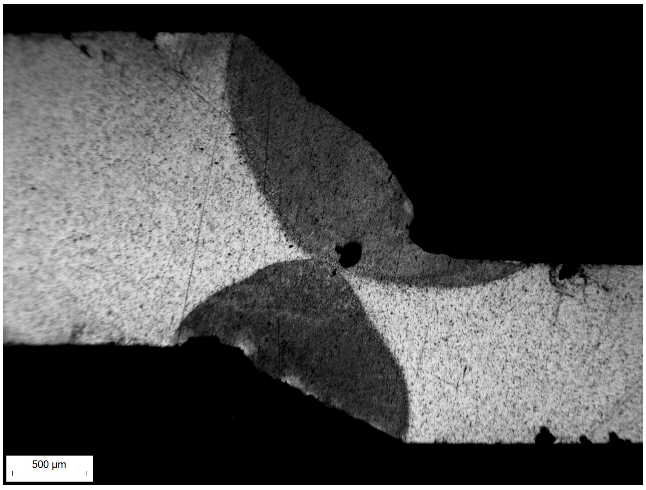


Figure 3.17: Example of a microscope observation (2x magnification of the 5754AA)

# Chapter 4

# Results Analysis

## 4.1 Results analysis EN AW 5754

### 4.1.1 Taguchi responses for Tensile test 5754 alloy

**Response Table for Means**

| Level | P (W) | V (m/min) | F (mm) |
|---|---|---|---|
| 1 | 109,7 | 140,1 | 135,9 |
| 2 | 131,6 | 129,8 | 127,5 |
| 3 | 142,0 | 113,5 | 119,9 |
| Delta | 32,3 | 26,6 | 16,1 |
| Rank | 1 | 2 | 3 |

Figure 4.1: 5754 alloy Response table for means Tensile test

An initial analysis of the results was conducted through Minitab. The mean is the average response for each combination of control factor levels in a static Taguchi design. Depending on the response, the goal is to determine factor levels that either minimize or maximize the mean. Minitab calculates a separate mean for each combination of control factor levels in the design. Delta is the difference between the highest and lowest average response values for each factor. Minitab assigns ranks based on Delta values; Rank 1 to the highest Delta value, Rank 2 to the second highest, and so on, to indicate the relative effect of each factor on the response. So, from the table in fig. 4.1 can be deducted that the laser power has the largest effect on the means, followed by the welding speed.

Now, in order to determine whether the association between the response and each term in the model is statistically significant, the p-value for the term must be compared to a significance level to assess the null hypothesis. The null hypothesis is that the term's coefficient is equal to zero, which implies that there is no association between the term and the response. Usually, a significance level (denoted as alpha $\alpha$) of 0.05 works well. A significance level of 0.05 indicates a 5% risk of concluding that an association exists when there is no actual association. The p-value results to be too

**Analysis of Variance for Means**

| Source | DF | Seq SS | Adj SS | Adj MS | F | P |
|---|---|---|---|---|---|---|
| P (W) | 2 | 1630,6 | 1630,6 | 815,3 | 0,49 | 0,669 |
| V (m/min) | 2 | 1081,4 | 1081,4 | 540,7 | 0,33 | 0,753 |
| F (mm) | 2 | 387,8 | 387,8 | 193,9 | 0,12 | 0,895 |
| Residual Error | 2 | 3297,2 | 3297,2 | 1648,6 | | |
| Total | 8 | 6397,0 | | | | |

Figure 4.2: 5754 Analysis of variance for means Tensile test

high, which means that there isn't an association between the tensile test results and the welding parameters. This could be due to the fact that an optimal set of parameters was selected from which the welding parameters were varied, not obtaining statistically significant results from the analysis performed on Minitab.

### 4.1.2 Taguchi responses Erichsen test 5754 alloy

**Response Table for Means**

| Level | P (W) | V (m/min) | F (mm) |
|---|---|---|---|
| 1 | 2,918 | 3,254 | 2,996 |
| 2 | 3,766 | 3,182 | 3,210 |
| 3 | 3,285 | 3,532 | 3,762 |
| Delta | 0,848 | 0,350 | 0,766 |
| Rank | 1 | 3 | 2 |

Figure 4.3: 5754 alloy Response table for means Erichsen test

**Analysis of Variance for Means**

| Source | DF | Seq SS | Adj SS | Adj MS | F | P |
|---|---|---|---|---|---|---|
| P (W) | 2 | 1,0855 | 1,0855 | 0,5428 | 2,99 | 0,251 |
| V (m/min) | 2 | 0,2046 | 0,2046 | 0,1023 | 0,56 | 0,640 |
| F (mm) | 2 | 0,9369 | 0,9369 | 0,4684 | 2,58 | 0,279 |
| Residual Error | 2 | 0,3629 | 0,3629 | 0,1815 | | |
| Total | 8 | 2,5899 | | | | |

Figure 4.4: 5754 alloy Analysis of variance for means Tensile test

### 4.1.3 Metallographic analysis results 5754 alloy

In this section, macrographs of the weld bead cross-sections are presented in order to identify the relationship between the quality and shape of the joint obtained and the parameters used during the welding process. In the figure 4.5 the microstructure of the welded joint can be appreciated: here it is easy to distinguish the base material (BM), the heat affected zone (HAZ) and the welded zone (WD). *Köse (2016)* observed that the weld metal of joints as well as grain size of HAZ and the phases that formed were influenced by the thermal weld cycle.

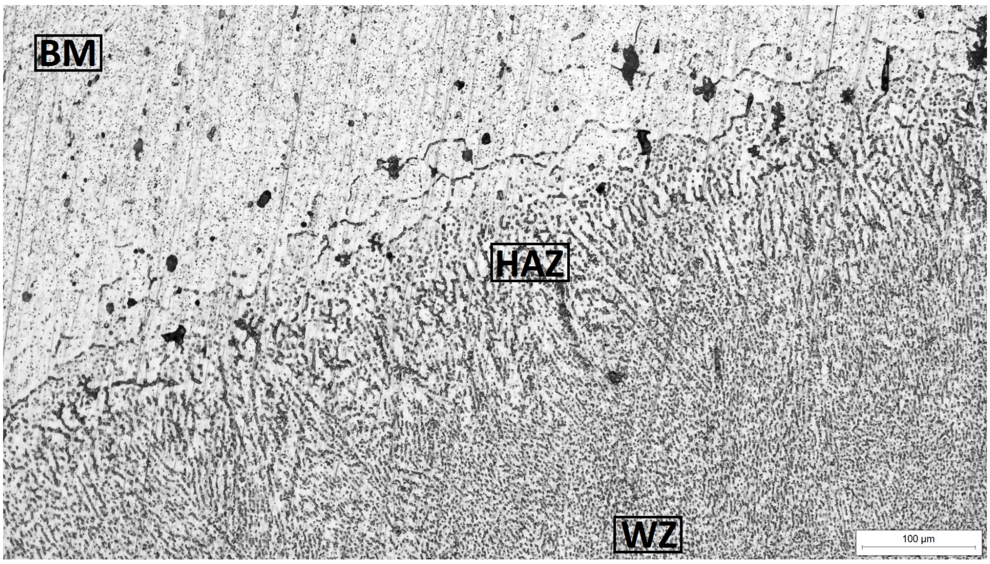


Figure 4.5: HAZ and weld metal microstructure image of the 5754 alloy (20x magnification

Macrographic observations of the weld cross-sections obtained from observation with optical microscope are now reported. It is known that the form of the weld pool, cooling rates, weld metal and HAZ microstructure are related to heat input during the welding process [23]. The analysis of these results will aid in better interpretation of the results obtained from the Tensile test and the Erichsen test. To highlight the effect that welding process parameters have on the joint, the specimens were divided according to the power level used and the effects that varying the focal distance and speed have on the welded joint were observed. It is important to note that for the 5754 alloy, the welded joints were obtained by means of two welding passes: the first pass is the upper one, while the second, obtained by turning the sheet over, is the lower one.

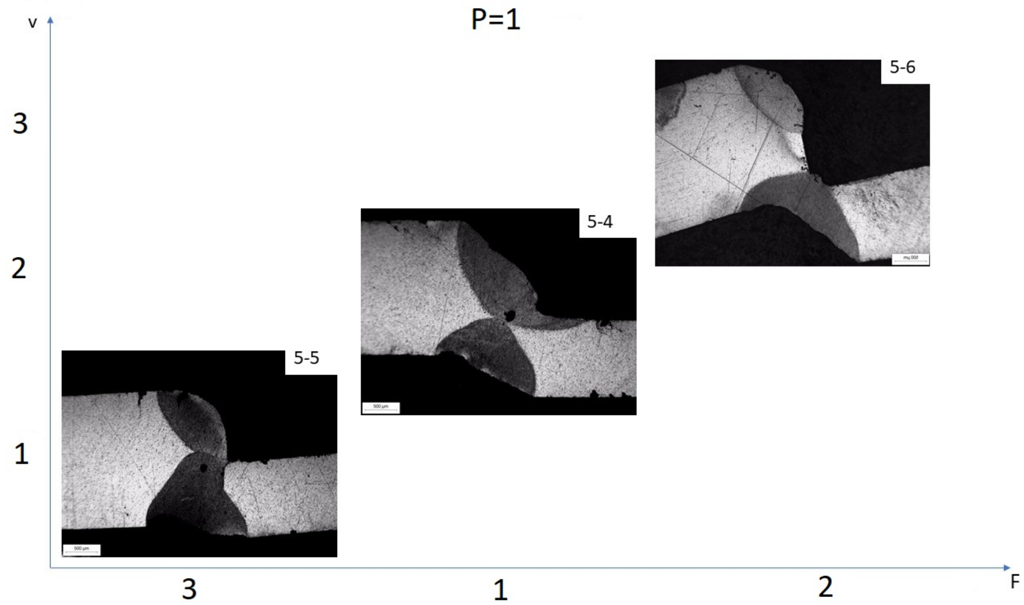


Figure 4.6: Lowest laser 5754 alloy

In figure 4.6 the power is kept fixed at the lowest value, in the y-axis is reported the speed and in the x-axis is reported the focal length. It must be noticed that it has not been possible to organize the graph by increasing values of the focal distance, because the chosen DOE does not include all combinations of parameters. Looking at the sample 5-6 it is evident how, at a low power and an high speed it's not possible to melt enough material to get a proper joint, also getting poor penetration. Observing the sample 5-5 you can see that the width of the joint has not changed much with a small variation of the focal distance. However, using a lower speed the thermal contribution is greater, obtaining a good penetration and therefore a well formed joint. In the sample 5-4 it can be seen that an higher focal distance leads to a wider joint, and increasing the speed with respect the 5-5, a lower penetration has been obtained. Visible defects are present in samples 5-4 and 5-5. In samples 5-4 and can be observed a defect named *Negative mismatch* [1] whose scheme is shown in figure. The two sheets are not perfectly aligned on the bottom side, but the thin sheet is lower than the ideal condition.

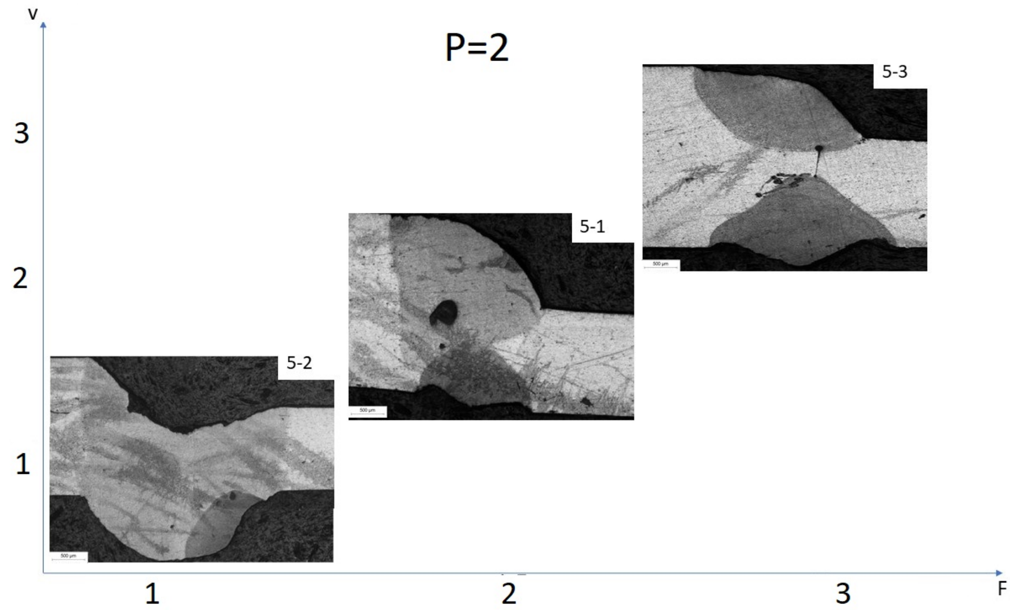


Figure 4.7: Intermediate power 5754 alloy

In the graph in figure 4.7 all the joints obtained with a intermediate power have been considered. In the specimen 5-1 it is evident how an higher power with a lower speed caused an excessive amount of material to melt, which consequently sank to the opposite side: this defect is identified by EN 10359:2015 standard as *weld sagging* (fig. 4.11) [1].

Using a focal length at level 2 a good result has been obtained (5-1). Despite some impurities are present, the joint seems to be well formed and a good penetration has been obtained. In the specimen 5-3 the defect of lack of penetration is present: this may be due to the higher speed combined with an higher focal length, which resulted in a wider but shallower joint.

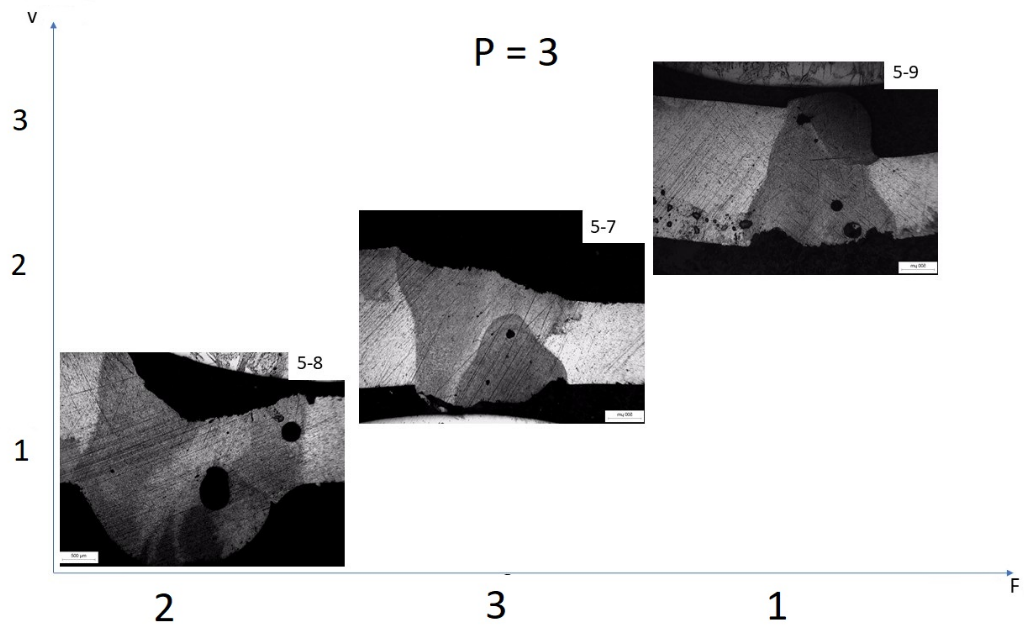


Figure 4.8: Highest power 5754 alloy

Using the highest power level it is possible to notice that in all three cases there has been complete melting of the material and the use of two passes seems to have been superfluous. In the 5-9 a good joint was obtained in spite of some impurities. In the 5-8 the use of a low speed produced the defect of *weld sagging*, and some impurities are also presents. From this microscopic inspection the 5-7 seems to be the best joint, where the keyhole formation was achieved. We reiterate how the use of a second welding pass seems to be unnecessary. In summary, the best welds appear to be those in samples 5-01, 5-07, 5-5 and 5-09. It is interesting to think in terms of *Heat Input HI (J/mm)* that can be measured as the ratio between the Power (W) and the speed (mm/s) (equation 3.1) and note that specimens 5-01, 5-05, 5-07, 5-09 have similar *Heat Input* values. In fact, regardless of the fire, which still has a fundamental influence on the quality of the joint, complete melting of the base material was achieved in these specimens. In the table 4.12 the values of the Heat Input (divided by the factor $x$) for these specimens are reported.

The weakest joints seem to be those of the samples 5-6 and 5-3. With these observations in mind, the results of the tensile test and the Erichsen test will be analyzed.

| Specimen | Heat Input HI (J/mm) | Focal length (Taguchi level) |
|---|---|---|
| 5-01 | 7.88 | 2 |
| 5-05 | 8.94 | 3 |
| 5-07 | 8.85 | 3 |
| 5-09 | 6.93 | 1 |

Table 4.1: Heat Input values for specimens 5-01, 5-05, 5-07, 5-09

### 4.1.4 Welding defects analysis 5754 alloy

As seen in the previous section, the defects that can be noted are: lack of penetration, weld sagging, negative mismatch and porosity.

In the literature, it is indicated that hydrogen-related macro and micro pore formations might develop during the laser welding process related to high cooling regime [12], [10], [28]. Several cases of porosity formation were found in this study. It is known that porosity formation can be minimized by controlling the solidification process using a pulsed current during the welding process. In this study, all the joints are formed by means of a continuous laser wave, this could explain the formation of porosity in most joints. An example of porosity defect is depicted in picture 4.9.

The lack of penetration defect when only part of the material is melted, not resulting in a complete weld joint. It is possible to observe this type of defect in the figure 4.10.

The European standard UNI EN 10359:2015 establishes deviation values $h$, above which *weld sagging* and *negative mismatch* defects compromise the quality of the tailor blank.

In particular, with reference to figures 4.11 and 4.12:

*Weld sagging (only for $t_2 > 1mm$)*

$$h \leq 0.1 \times t_2 \; mm \tag{4.1}$$

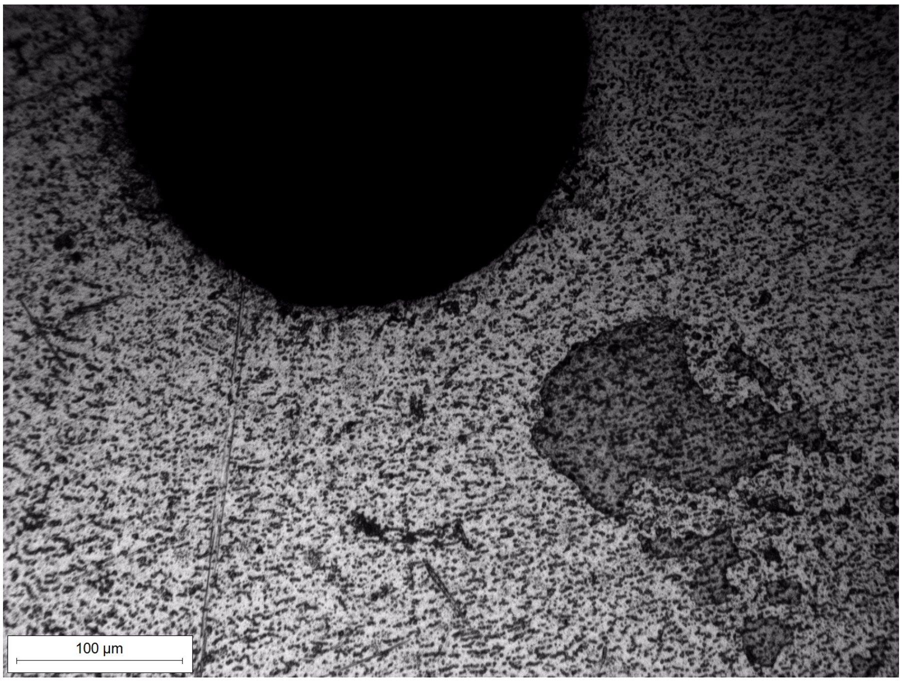


Figure 4.9: Porosity defect 5754 alloy

Where $t_2$ is the thickness of the thinner sheet.

*Negative mismatch (only for $t_2 > 1mm$)*

$$h \leq 0.1 \times t_2 \; mm \tag{4.2}$$

Where $t_2$ is the thickness of the thinner sheet.

In the case of this research, the sheet of smaller thickness has a value of $t_2 = 1.2mm$, so:

$$0.1 \times t_2 = 0.1 \times 1.2 = 0.12 \; mm \tag{4.3}$$

In order to measure the values of interest was used the software *ImageJ*. Importing the micrograph of interest in the software, it is possible to calibrate the same by entering the measures already known: measuring the thickness of the sheets (2mm and 1.2mm) or using the scale bar generated by the microscope software.

The figure 4.13 shows the micrographic image of the sample 5-02, with the measurements of the *weld sagging* defect. As it was already clear from a first observation, the weld sagging defect is very marked and exceeds the limits imposed by the standard.

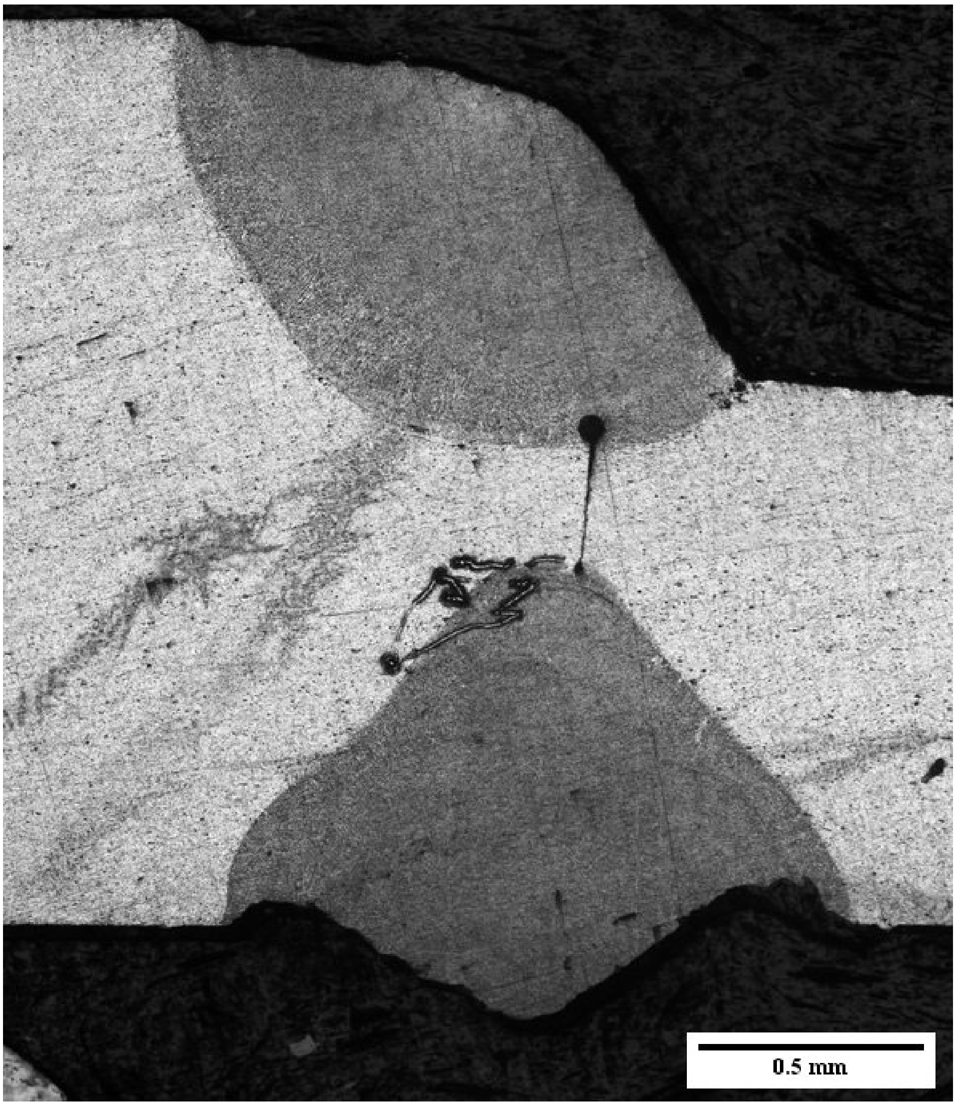


Figure 4.10: Specimen 5-03, lack of penetration

Also specimen 5-08 (fig. 4.13) shows a weld sagging defect, and also some porosity defects, which also exceed the limits imposed by the European standard.

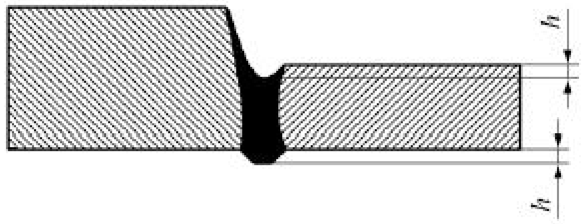


Figure 4.11: Weld Sagging defect

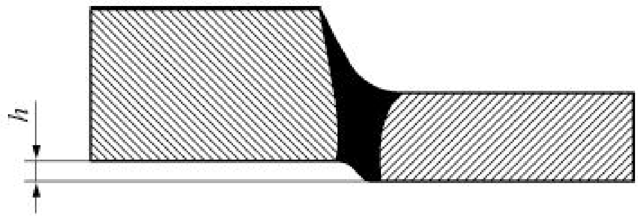


Figure 4.12: Negative mismatch

The *negative mismatch* defect involves a misalignment of the two sheets following the welding process. This defect was found in specimens 5-06 and 5-04. As predicted in sample 5-04 (figure 4.15) the deviation h exceeds the maximum values imposed by the standard.

A measurement of the misalignment in test specimen 5-06 would be superfluous, as one can only be certain of the defect by visual inspection.

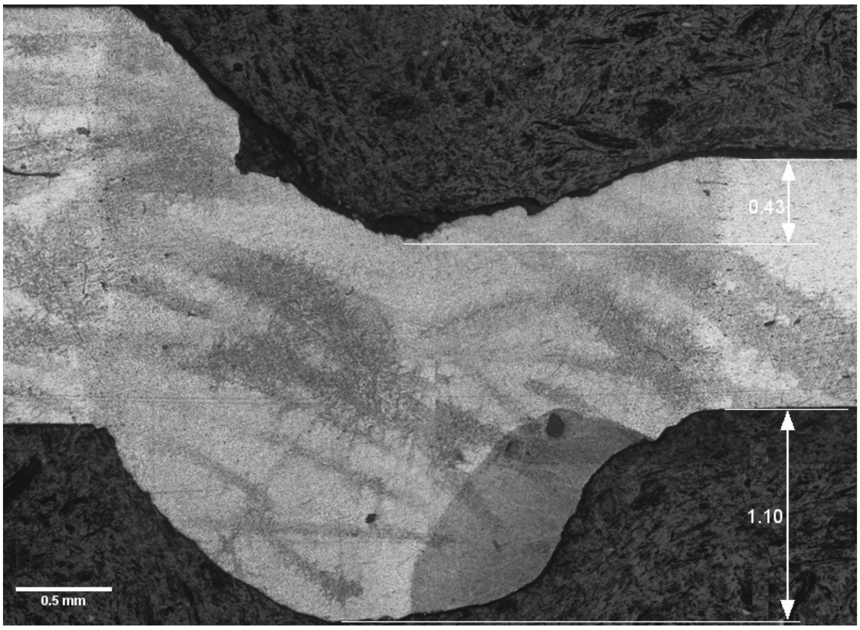


Figure 4.13: Specimen 5-02, weld sagging defect (2x magnification)

Finally, it is interesting to observe the defects present in welded specimen 5-07. As previously mentioned, in this specimen the keyhole was obtained, a sign of good welding. However, the use of a second pass of welding resulted in porosity defects, leading to a weakening of the specimen. Moreover, the mismatch between the two sheets is within the limits of European standards, despite the imperfect welding. However, this measure should not be attributed significant weight due to the use of a double pass, which led to excessive deformation of the sheets. The micrographic image of test specimen 5-07 is therefore reported in figure 4.16.

### 4.1.5 Tensile test results 5754 alloy

The results of the tensile test are reported on the table 4.2, where the acronym *W* indicates that the rupture occurred on the welded joint, while the acronym *BM* indicates that the rupture is on the base material. Three tensile specimens were obtained from each metal sheet, so that there were three replicates of the same test. It should be noted that the test specimen relating to test 1 is the one closest to the weld seam connection (see fig.3.5).

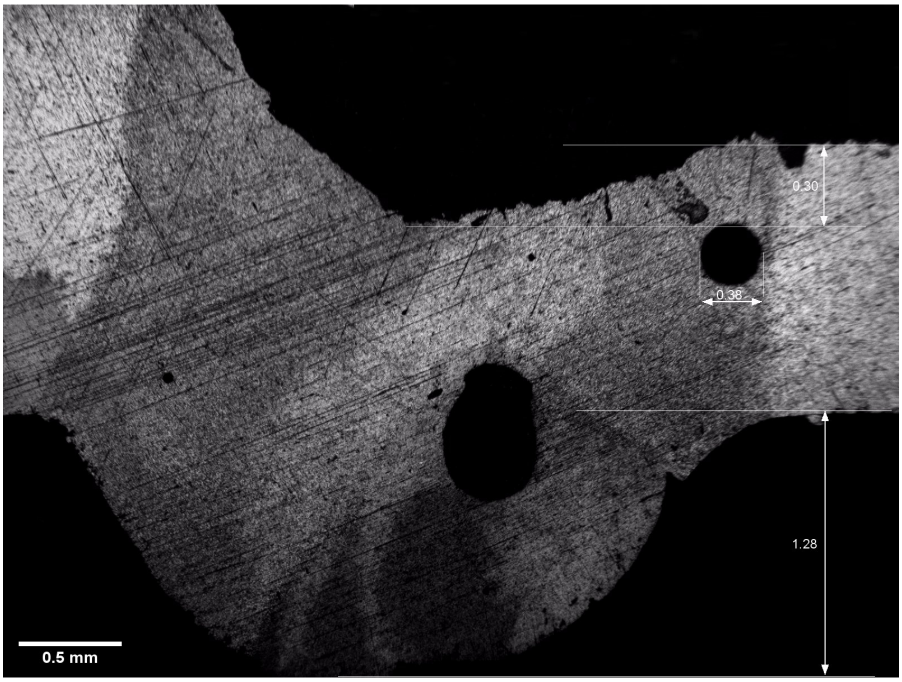


Figure 4.14: Specimen 5-08, weld sagging and porosity defects (2x magnification)

Samples 5-1, 5-5 and 5-9 which were found to be among the best by microscopic observation are the only ones that reported a break in the base material indicating good joint strength. These three specimens also have the highest breaking loads. Despite one of the replicas present a poor result, even the specimen 5-7 have a breaking load quite high. As predicted by microscopic observation the joints 5-3 and 5-6 have low breaking loads: remember that in 5-6 a small joint was observed, while in 5-3 a lack of penetration defect was observed. Even the 5-4, which was found not to have a total material melt, shows a rather low load. 4.3.

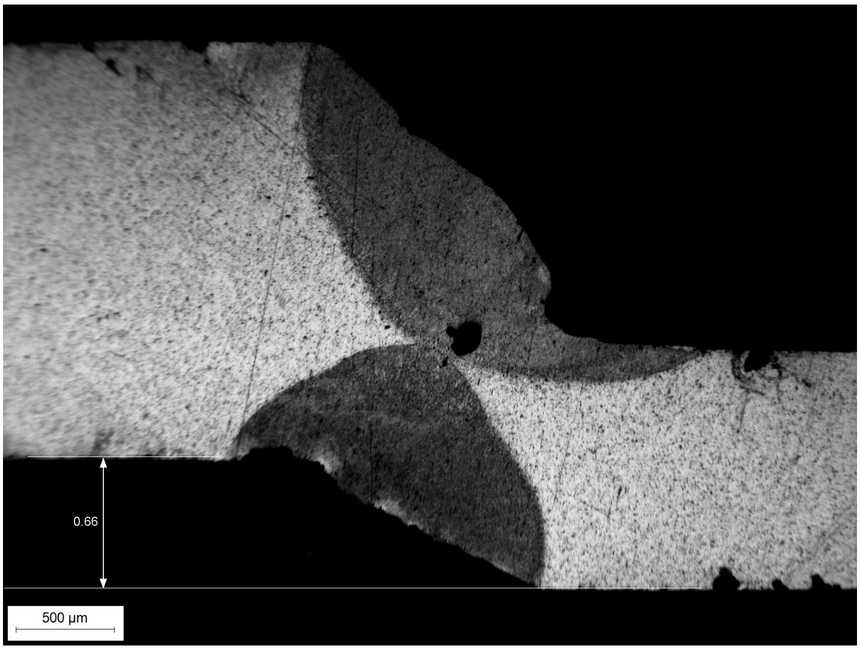


Figure 4.15: Specimen 5-04, negative mismatch defect (2x magnification)

The mean value, standard deviation and COV of the tensile test results have been calculated and are reported in the table 4.3. The specimens highlighted in the table are those that presented the best results in the tensile test. Specimens with the highest maximum load values and lowest have been highlighted in green. Observing these results, it can be seen that the bead is homogeneous throughout its length, indicating a good welding process. The specimens highlighted in orange are those that, despite having reported good values in terms of maximum load, have very high COVs %. This indicates non-uniformity along the weld bead. In particular, looking at the table 4.2, it can be seen that for test specimens 5-07 and 5-05 the lowest value of the three test replicates is that for test 1 (i.e. the specimen closest to the welding attachment point). Another observation to be made is that the specimens highlighted in green have suffered breakage on the base material on at least one of the three replicas, while the specimens highlighted in orange have suffered breakage only on the base material.

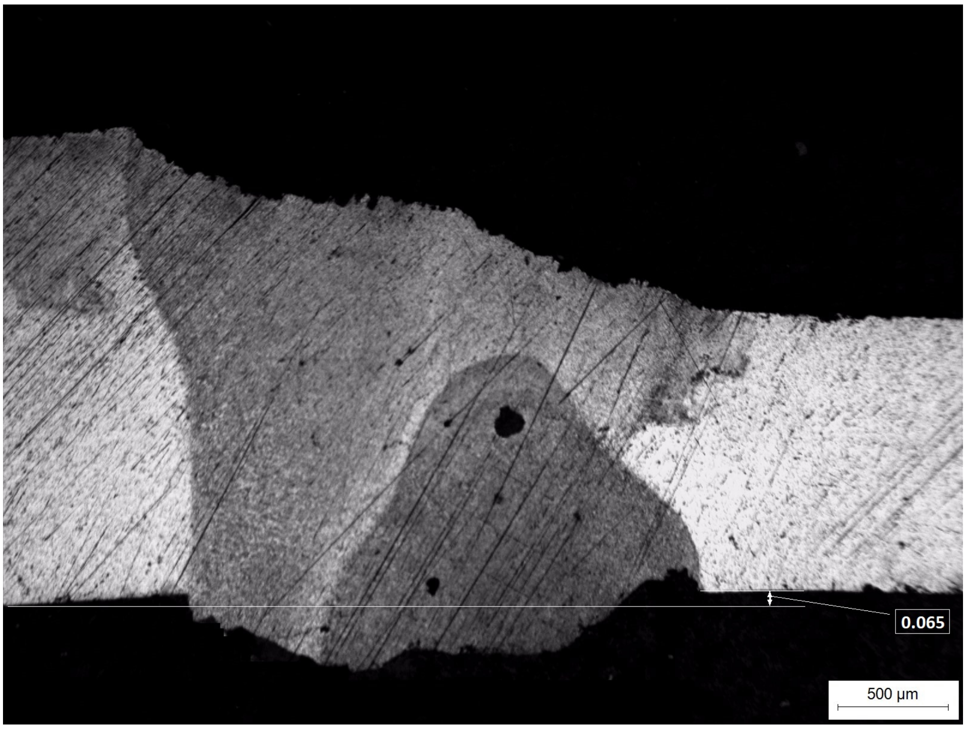


Figure 4.16: Specimen 5-07, keyhole (2x magnification)

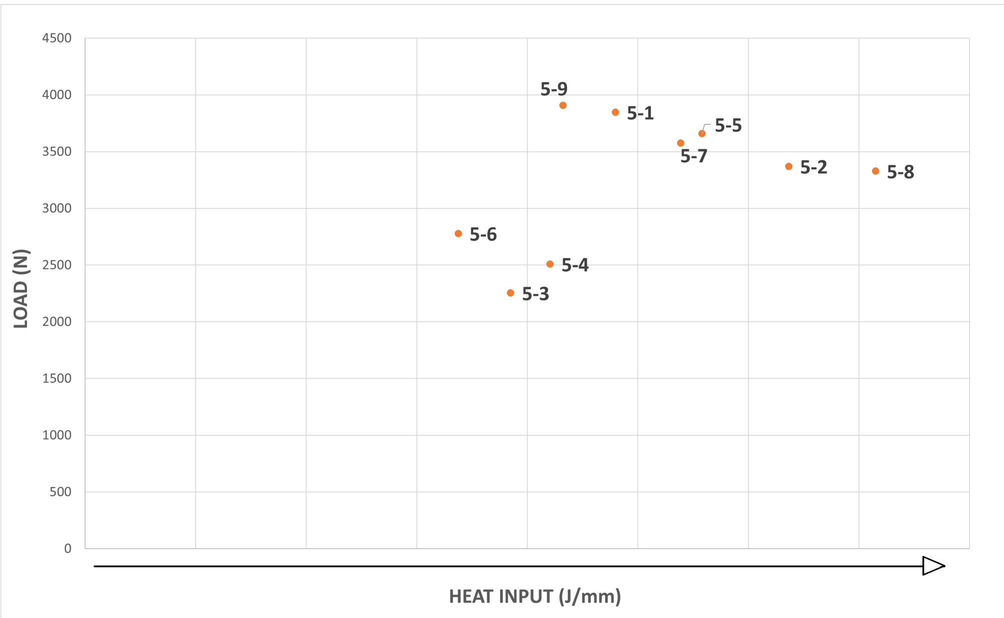


Figure 4.17: Tensile test results versus Heat Input, 5754 alloy

| Specimen | Test 1 | | Test 2 | | Test 3 | |
|---|---|---|---|---|---|---|
| | Crack | LOAD (N) | Crack | LOAD (N) | Crack | LOAD (N) |
| 5-01 | W | 3935 | BM | 3997 | BM | 3611 |
| 5-02 | W | 3232 | W | 3665 | W | 3215 |
| 5-03 | W | 2406 | W | 2209 | W | 2148 |
| 5-04 | W | 2298 | W | 2594 | W | 2634 |
| 5-05 | W | 2842 | W | 3640 | W | 3678 |
| 5-06 | W | 460 | W | 2583 | W | 2976 |
| 5-07 | W | 1822 | W | 3639 | W | 3509 |
| 5-08 | W | 3388 | W | 3240 | W | 3358 |
| 5-09 | W | 3948 | BM | 3910 | W | 3869 |

Table 4.2: Tensile load and point of fracture 5754 alloy

Finally, the results of the tensile test as a function of *heat input* are analyzed to confirm the relationship between the joint obtained and its tensile strength. From the graph in the figure 4.17 it can be seen that the best welds were obtained with a heat input between a certain range. Outside this range there are welded joints that have resisted less in the tensile test. It would therefore seem that this would be the optimal range to obtain good results. It should be noted that in this range there is also sample 5-4, which however has a low breaking load: this could be due to the fact that the focal distance of 1 mm was not sufficient to obtain a joint with adequate penetration. It is interesting to note that specimens 5-2 and 5-8 also show good tensile strength, but still lower than the maximum values observed for the other welds. In fact, these specimens, being outside the previously defined range, presented the welding defect of sagging. The curve obtained during the tensile test of sample 5-1 is shown in the figure 4.18. It can be seen that the specimen presents a small elongation after reaching the maximum load, after which, as soon as the fracture occurs the load drops immediately, breaking in the base material.

| Specimen | Mean (N) | Standard Deviation (N) | COV% |
|---|---|---|---|
| 5-01 | 3847,5 | 207,2 | 5,4 |
| 5-02 | 3371,0 | 255,0 | 7,6 |
| 5-03 | 2254,5 | 135,1 | 6,0 |
| 5-04 | 2508,5 | 183,4 | 7,3 |
| 5-05 | 3386,6 | 471,7 | 13,9 |
| 5-06 | 2006,0 | 1353,3 | 67,5 |
| 5-07 | 2990,1 | 1013,8 | 33,9 |
| 5-08 | 3328,6 | 78,1 | 2,3 |
| 5-09 | 3908,9 | 39,4 | 1,0 |

Table 4.3: Mean value, SD, COV of tensile load values for 5754 alloy

While as you can see from the figure 4.19, the specimen 5-8 shows a slightly different behavior: once the maximum load is reached, the specimen did not show an evident elongation and the load drops suddenly as the fracture appears. Remember how this sample broke in the welded joint.

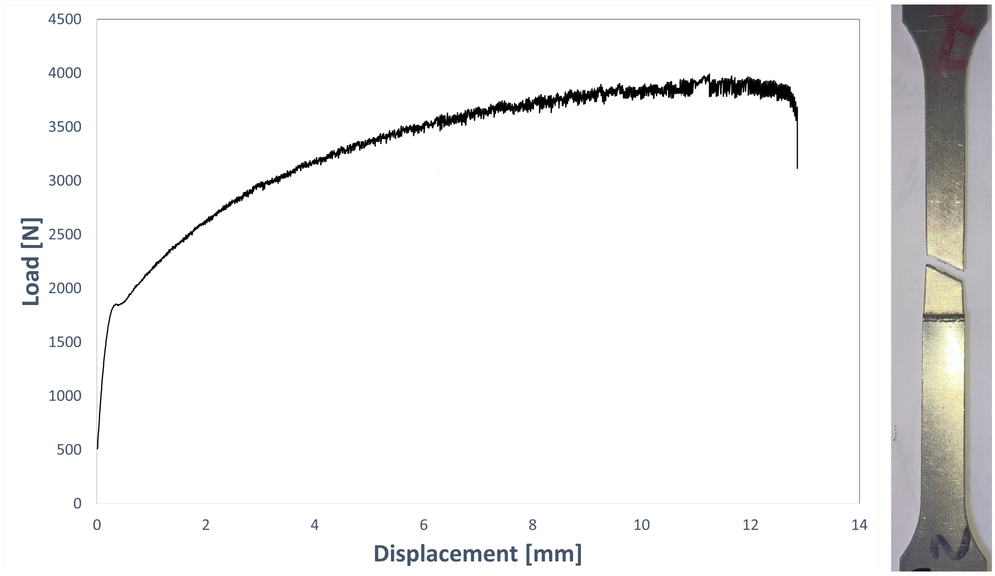


Figure 4.18: Tensile test curve of the sample 5-1 and the specimen with rupture in the base material

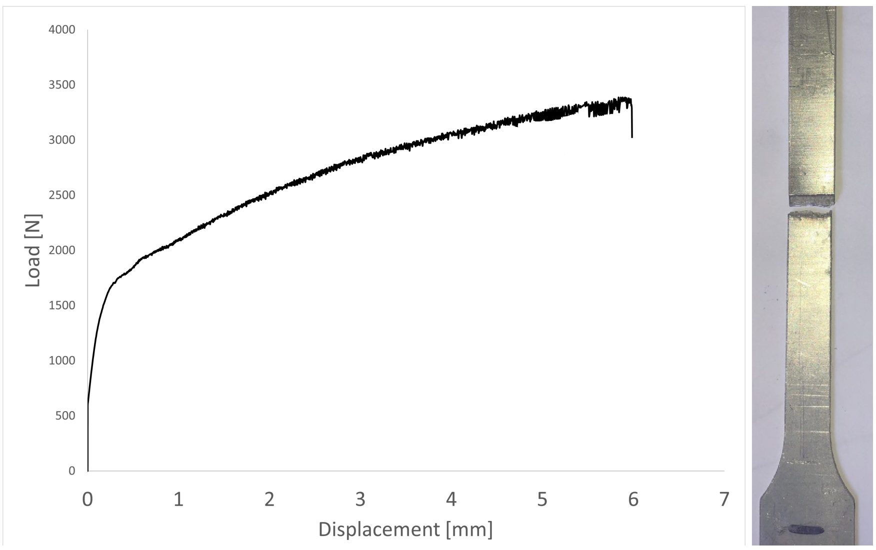


Figure 4.19: Tensile test curve of the sample 5-8 and the specimen with rupture in the welded joint

### 4.1.6 Erichsen cupping test results 5754 alloy

The results of the Erichsen cupping test are now analyzed. The values output to the test are the *Erichsen index EI (mm)*, which indicates how far the punch has fallen by deforming the specimen and the load applied. In the table 4.4 the results of the the results of the three replications are reported, where test 1 is referred to the specimen closest to the end of the weld bead. In table 4.5 the values of mean value, standard deviation and coefficient of variation are reported.

Let us first consider the specimens that returned the best results in the metallographic analysis and in the tensile test: 5-01, 5-05, 5-07, 5-09. The specimen 5-01 broke in all three replications on the base material, reporting an average $EI = 3.7mm$. The specimen 5-05 did not produce optimal results, in fact the welded joint always broke and the Erichsen index values were rather low. Note how the values increase as you move away from the end of the weld seam. The specimen 5-07, although it did not have the highest Erichsen index values, suffered fracture in the base material in the test specimen cut at a greater distance from the end of the weld seam. The specimen 5-09 broke on the base material and reported low EI values. From the evaluations just performed, it is possible to state that good tensile strength of the joint does not imply good formability. However, it is clear how outliers due to human error during the conduct of the test must be accounted for. The specimens that returned the best results in the Erichsen cupping test are: 5-01, 5-03, 5-05, 5-08. It has been observed by metallographic analysis that specimen 5-03 has an evident welding defect: lack of penetration. For this reason it is necessary to exclude it from future analysis as it is surely an outlier. Considering also that specimen 5-08 had a significant weld sagging defect,and therefore had a poor quality joint, this should also be excluded from future analysis.

However, it can be seen in the table 4.5 that all COV values are quite high, indicating a lack of homogeneity along the weld seam. The problem of data scatter in the Erichsen test was similarly encountered by *Bergamo S* [7]. This could be due to several factors. As mentioned before, due to human error in specimen placement, set

| Specimen | Test 1 | | Test 2 | | Test 3 | |
|---|---|---|---|---|---|---|
| | Crack | EI (mm) | Crack | EI (mm) | Crack | EI (mm) |
| 5-01 | BM | 4,0 | BM | 3,0 | BM | 3,4 |
| 5-02 | W | 2,9 | W | 3,1 | BM | 3,4 |
| 5-03 | W | 3,2 | W | 6,0 | W | 4,8 |
| 5-04 | W | 3,4 | W | 2,2 | BM | 2,5 |
| 5-05 | W | 2,7 | W | 2,7 | W | 4,4 |
| 5-06 | W | 1,8 | W | 2,8 | W | 3,8 |
| 5-07 | W | 2,5 | W | 3,5 | BM | 4,1 |
| 5-08 | W | 3,5 | W | 3,3 | W | 3,3 |
| 5-09 | W | 2,3 | W | 3,8 | W | 3,3 |

Table 4.4: Erichsen Index's and Point of fracture 5754 alloy

of the zero of the punch and/or tightening of the bolts. A second factor that may have contributed to amplifying the variability of the data compared to tensile testing is the larger size of the specimens and the resulting greater distance between measurement points. The third factor that is believed to have increased the dispersion of the Erichsen Indices is the misalignment of the plates, which was already observed in some of the metallographic analysis and was found to be a critical aspect of the experimental campaign.

Similarly to what has been done for the tensile test, the graph in the figure 4.20 shows the results of the Erichsen test as a function of *Heat input HI*. In microscopic observations and tensile tests, an optimal heat input range was identified. From the graph in figure 4.20 you can see that specimen 5-03, 5-06, 5-02 and 5-08 are outside this range. If we exclude the sample 5-03, which is considered an outlier, the samples previously identified are those that gave the best results.

By way of example, the graph obtained from the Erichsen cupping test of sample 5-09 is shown in figure 4.21.

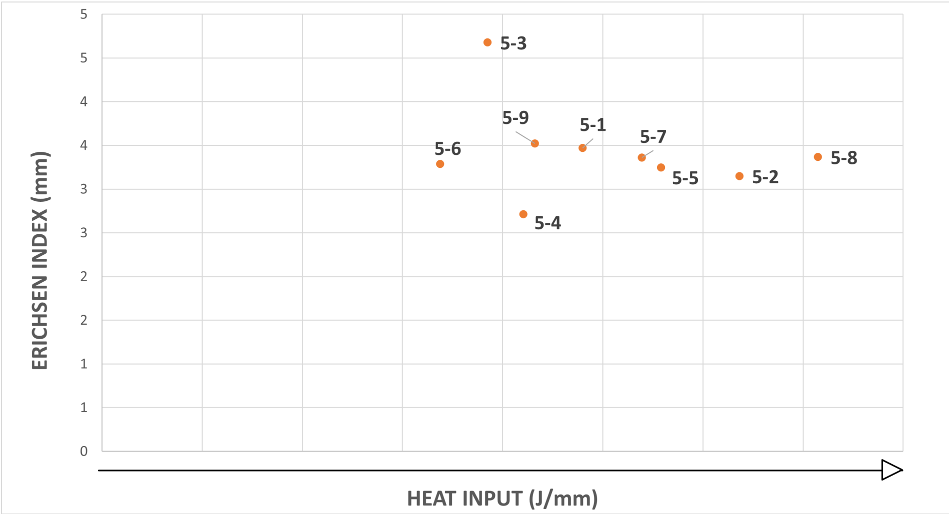


Figure 4.20: Erichsen test results versus Heat Input, 5754 alloy

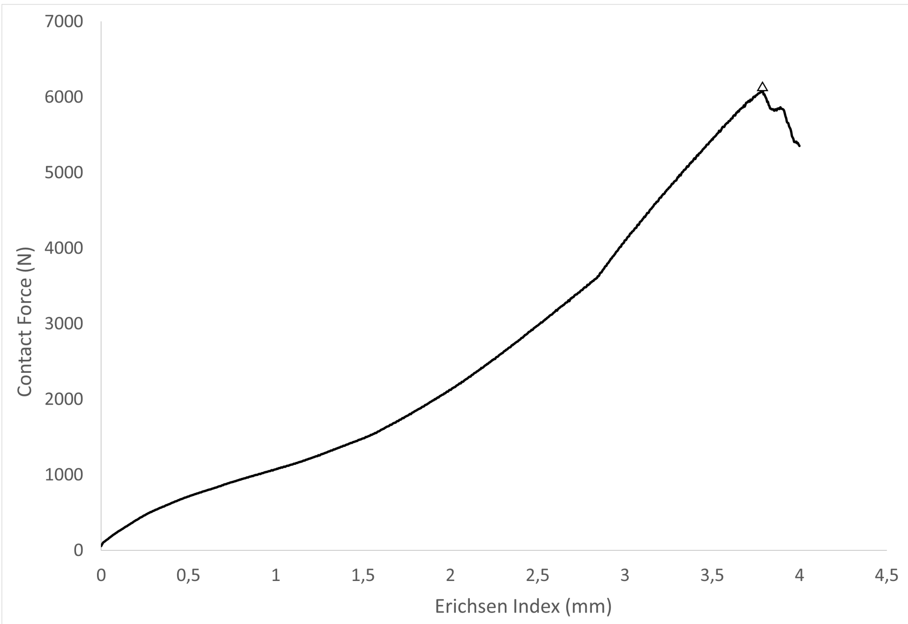


Figure 4.21: Erichsen cupping test curve

| Specimen | Mean (mm) | Standard Deviation (mm) | COV% |
|---|---|---|---|
| 5-01 | 3,7 | 0,5 | 13,5 |
| 5-02 | 3,2 | 0,2 | 7,8 |
| 5-03 | 4,0 | 1,4 | 34,7 |
| 5-04 | 3,0 | 0,6 | 20,0 |
| 5-05 | 3,5 | 1,0 | 28,3 |
| 5-06 | 2,8 | 1,0 | 35,9 |
| 5-07 | 3,3 | 0,8 | 24,2 |
| 5-08 | 3,4 | 0,2 | 4,6 |
| 5-09 | 2,8 | 0,7 | 26,2 |

Table 4.5: Erichsen Index's mean value 5754 alloy

### 4.1.7 Summary of the result analysis 5754 alloy

The performance in terms of maximum tensile load and EI for the 5754 alloy specimens is now reported. In order to observe which specimens returned better results in terms of both maximum load and Erichsen's index. From the graph in figure 4.22 we can see that the samples that have returned better values are 5-01 and 5-09. However, as observed in the metallographic analysis, these specimens exhibited several welding defects. These defects could be due to the failure to use shielding gas or the use of a welding fixing system that has yet to be perfected. Another very important factor that could have influenced the quality of the weld joint was the use of a double welding pass, where it was not necessary as a complete melting of the material had already been achieved. For ease of reading, the table 4.6 with the values of Heat input (J/mm) and Focal length (mm) is shown once again.

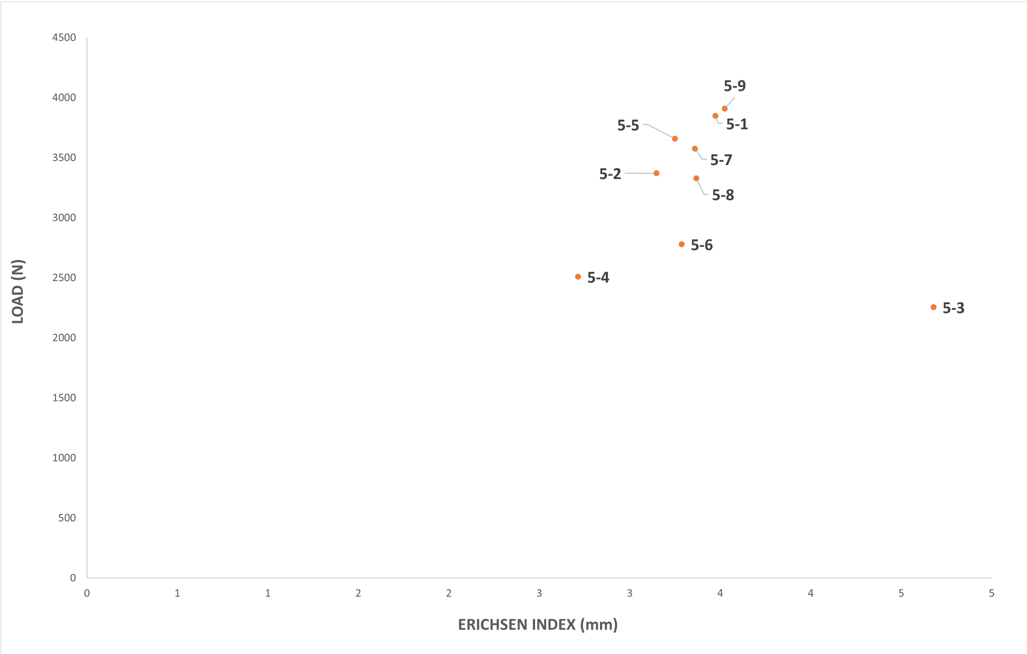


Figure 4.22: Maximum load versus Erichsen's index 5754 alloy

Specimens 5-05 and 5-07 also returned a good compromise in terms of maximum load and Erichsen index. In addition, it is recalled how good quality joints with few imperfections were obtained, and how in specimen 5-07 keyhole was obtained, despite some welding imperfections. Also here the use of the second pass turns out to be influential in a negative way. It is important to note that the highest quality joints are those in which there is a focal distance greater than 1 mm, thus concentrating the laser beam below the surface of both sheets which we remember to be 2 mm and 1.2 mm.

| Specimen | Heat Input HI (J/mm) | Focal length (Taguchi level) |
|---|---|---|
| 5-01 | 7.88 | 2 |
| 5-05 | 8.94 | 3 |
| 5-07 | 8.85 | 3 |
| 5-09 | 6.93 | 1 |

Table 4.6: Heat Input values for specimens 5-01, 5-05, 5-07, 5-09

## 4.2 Results analysis EN AW 6016

### 4.2.1 Taguchi responses 6016 alloy

The results of the analysis performed by minitab of the tensile tests and the Erichsen cupping test for aluminum alloy 6016 are now reported in tables in figures 4.23 and 4.24. Recall that in order to determine whether the association between the response and each model term (in this case power, velocity, and focal distance) is statistically significant, the p-value must be taken into account. Using a significance level $\alpha = 0.05$, it can be seen that for both the tensile test and the Erichsen test, the parameters are found to be not statistically significant. Although several attempts were made through model reduction, in which one parameter was excluded from the model at a time, the analysis still turns out to be unsuccessful. This finding, however, should not be considered negative. In fact, we recall how the welding parameters were selected from a set of optimal parameters already calculated by *Bergamo S. (2021)*. Therefore, moving within such a small range of parameters, it is not possible to appreciate a notable difference between the tests performed.

**Analysis of Variance for Means**

| Source | DF | Seq SS | Adj SS | Adj MS | F | P |
|---|---|---|---|---|---|---|
| P (W) | 2 | 168,77 | 168,77 | 84,39 | 2,63 | 0,275 |
| V(m/min) | 2 | 312,58 | 312,58 | 156,29 | 4,88 | 0,170 |
| F(mm) | 2 | 38,80 | 38,80 | 19,40 | 0,61 | 0,623 |
| Residual Error | 2 | 64,06 | 64,06 | 32,03 | | |
| Total | 8 | 584,20 | | | | |

Figure 4.23: 6016 alloy Analysis of variance for means Tensile test

**Analysis of Variance for Means**

| Source | DF | Seq SS | Adj SS | Adj MS | F | P |
|---|---|---|---|---|---|---|
| P (W) | 2 | 0,15749 | 0,15749 | 0,078745 | 0,47 | 0,679 |
| V(m/min) | 2 | 0,86318 | 0,86318 | 0,431591 | 2,60 | 0,278 |
| F(mm) | 2 | 0,01673 | 0,01673 | 0,008367 | 0,05 | 0,952 |
| Residual Error | 2 | 0,33241 | 0,33241 | 0,166207 | | |
| Total | 8 | 1,36982 | | | | |

Figure 4.24: 6016 alloy Analysis of variance for means Erichsen test

### 4.2.2 Metallographic analysis results 6016 alloy

Figure 4.25 shows a 20x magnification of a solder joint for Alloy 6016, in which the base material (BM), heat affected zone (HAZ) and melt zone (WZ) can be distinguished.

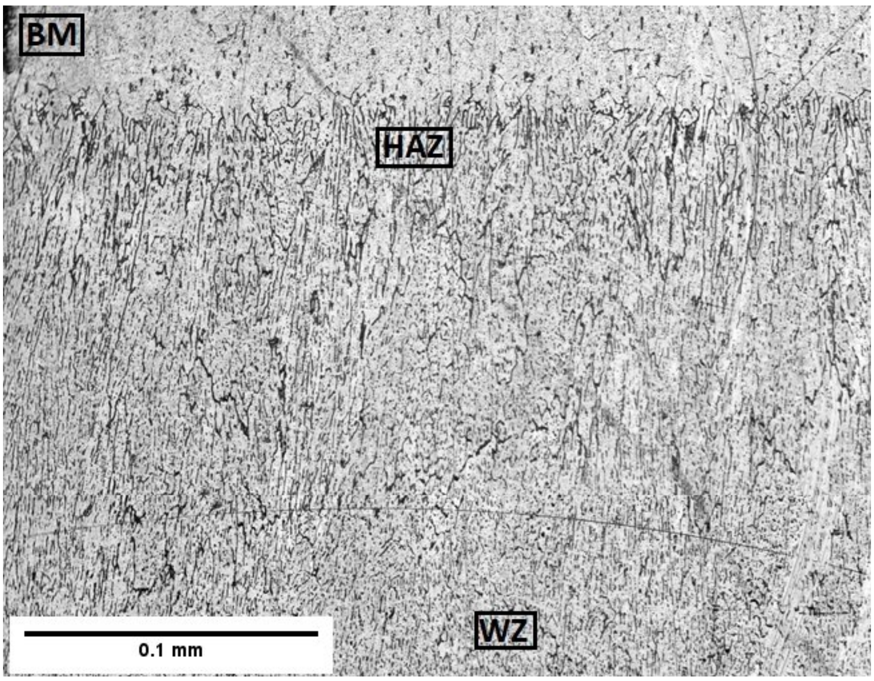


Figure 4.25: 20x magnification of the cross-section of a welded joint, 6016 alloy

Now, as done for alloy 5754, we now analyze the macrographs of the welded joints of alloy 6016 as the welding parameters change. In figures 4.26, 4.27 and 4.28 there are three different power levels, and welding speed (y axis) and focal distance (x axis) have been varied. It is specified that only one welding pass was used in the 6016 alloy welding operations. From a first observation no appreciable differences are noticed, and the geometry of the joints is quite homogeneous. This could be due to the fact that as seen in scientific literature [14], above a certain level of Heat Input the complete melting of the material is obtained. However, through the use of the software *ImageJ*, it is possible to measure the dimensions of the welded joint, so as to try to understand the influence of the parameters. An example of how the joint is measured with *ImageJ* is shown in the figure 4.29, while you can observe the rest of the measurements in the table 4.7. Even from this analysis, it is not possible to understand the link between the welding parameters and the joint geometry.

| Specimen | Heat Input (J/mm) | Focal Length (Taguchi level) | Joint width (mm) |
|---|---|---|---|
| 6-01 | 9.62 | 2 | 3,17 |
| 6-02 | 12.02 | 1 | 3,80 |
| 6-03 | 8.01 | 3 | 2,81 |
| 6-04 | 8.81 | 1 | 3,210 |
| 6-05 | 11.06 | 3 | 3,84 |
| 6-06 | 7.37 | 2 | 3,24 |
| 6-07 | 10.42 | 3 | 3,22 |
| 6-08 | 12.98 | 2 | 3,53 |
| 6-09 | 8.65 | 1 | 3,19 |

Table 4.7: Welded joint width, 6016 alloy

So, to be able to identify the best joints you can refer to the European standard *Laser welded tailored blanks - Technical delivery conditions* [1], observing defects in joints and measuring their extent.

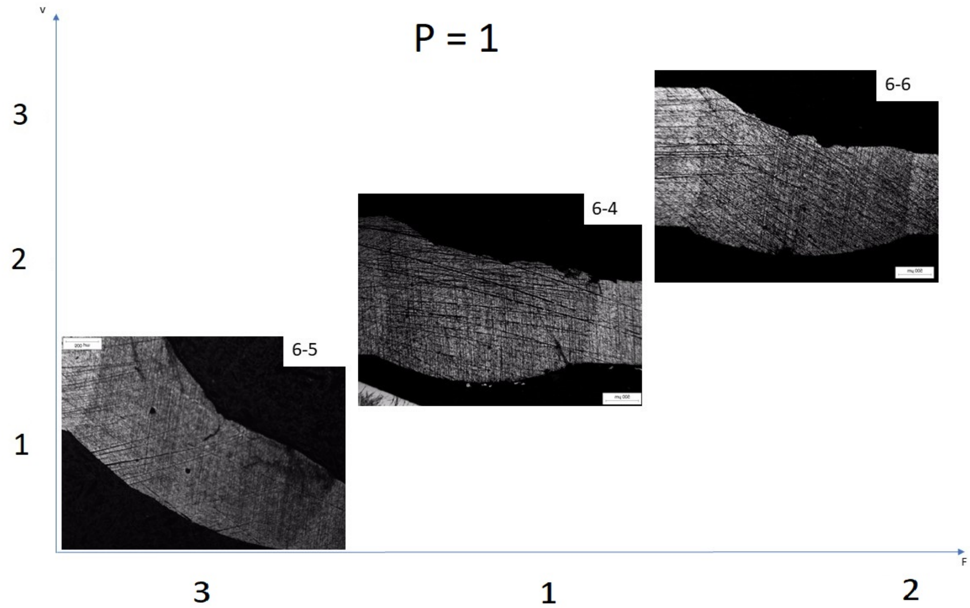


Figure 4.26: Lowest laser power 6016 alloy

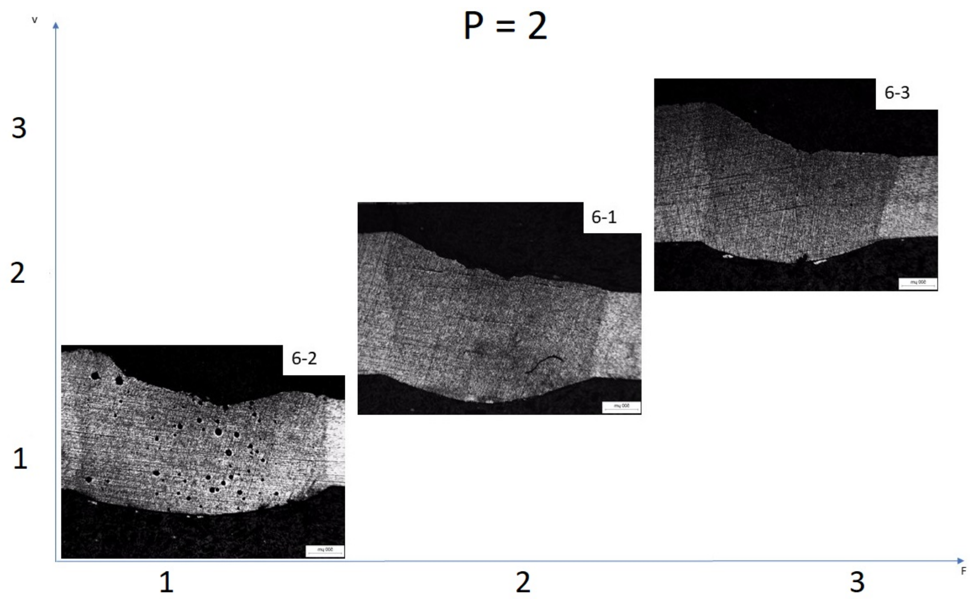


Figure 4.27: Intermediate laser power 6016 alloy

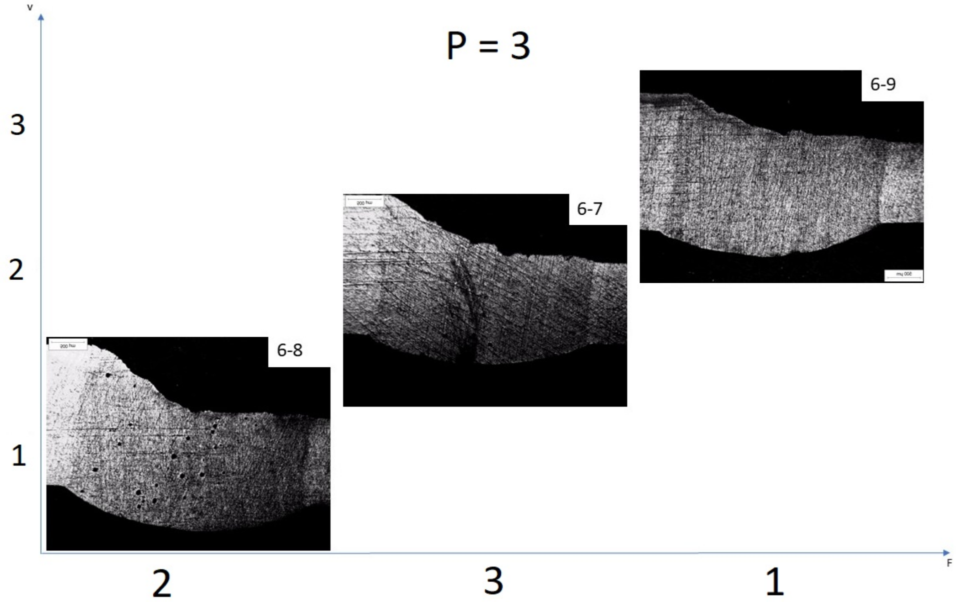


Figure 4.28: Highest laser power 6016 alloy

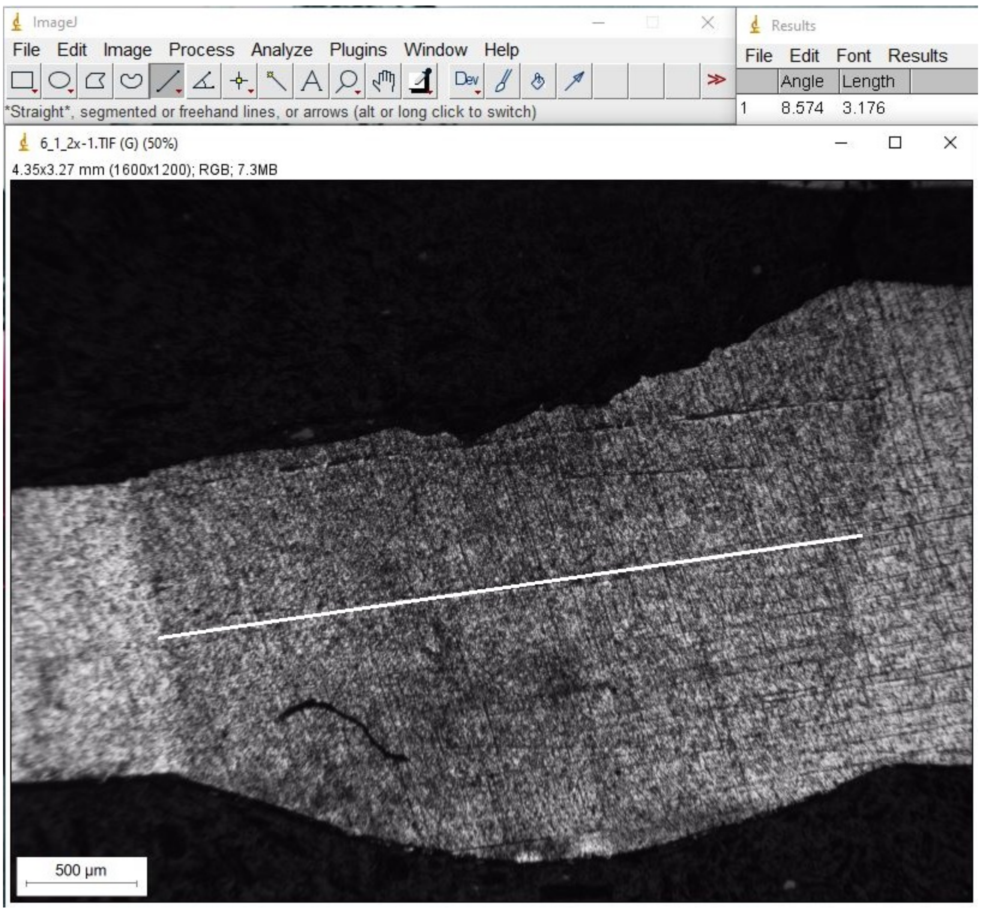


Figure 4.29: Measurement of the welded joint width using ImageJ

### 4.2.3 Welding defects analysis 6016 alloy

*Hot crack*: this defect (also called solidification cracks) starts to form once the metal reaches a temperature above the solidus temperature and the alloying elements with low melting point accumulate at grain boundaries. The area subject to solidification will be less ductile, and during cooling the weld metal will shrink, leading to crack formation. This type of defect in aluminum alloy welds has been extensively studied in the literature [27, 26], concluding that this defect occurs in most heat-treated 6xxx alloys. It would seem that one way to reduce cracks is to decrease the intensity of power and speed at the same time, thus decreasing the heat input to the metal but also the cooling ratio. This defect was manifested in test 6-01 where a power level 2 was used and test 6-05 with a power level 1, as we can see in the figure 4.30

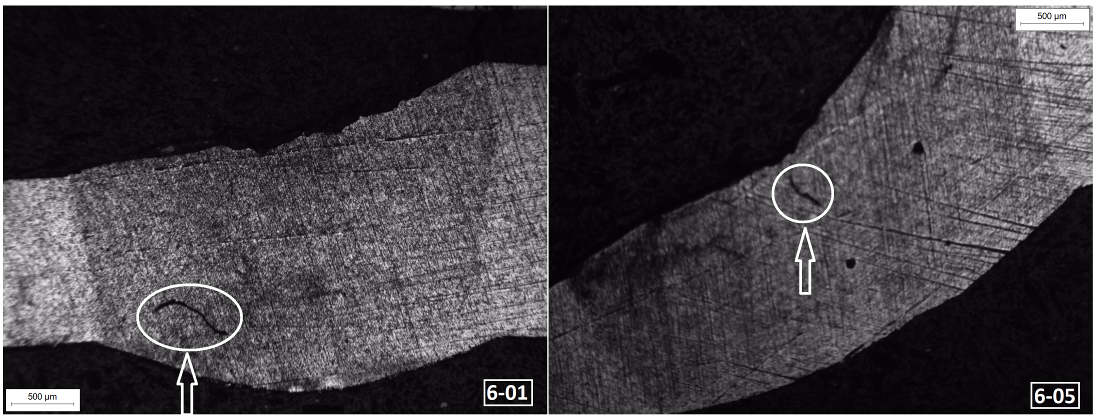


Figure 4.30: Hot crack defect in specimens 6-01 and 6-05

*Porosity*: As for the 5754 alloy, several cases of porosity defects have been found, with a density such as to make the welded joint unacceptable according to the European standard [1]. Figure 4.31 shows specimens 6-02 and 6-08 both affected by porosity.

*Excessive root penetration*: This defect may have occurred due to improper placement of the sheets, thus leaving too much space. As done previously for alloy 5754, the distance was calculated as prescribed by the standard using ImageJ software.

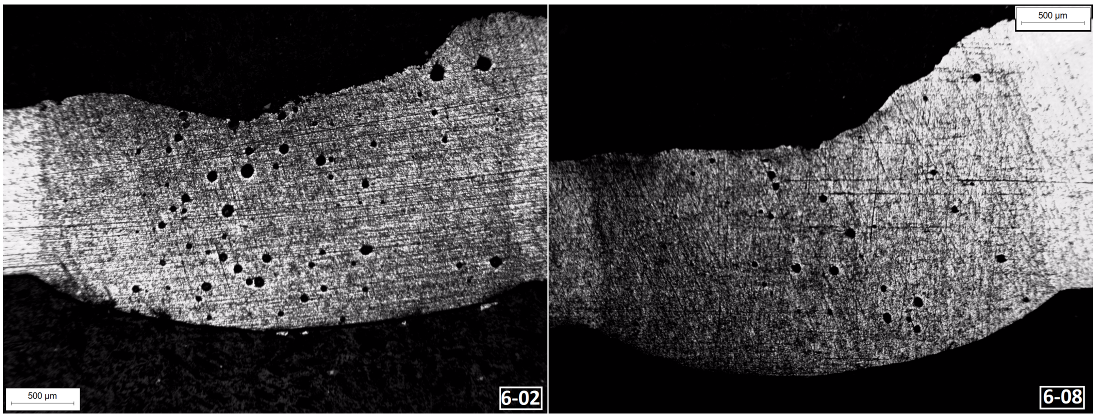


Figure 4.31: Porosity defect in specimens 6-02 and 6-08

This defect has been found in all 6016 alloy joints. The figure 4.32 shows an example of this type of defect on the specimen 6-03.

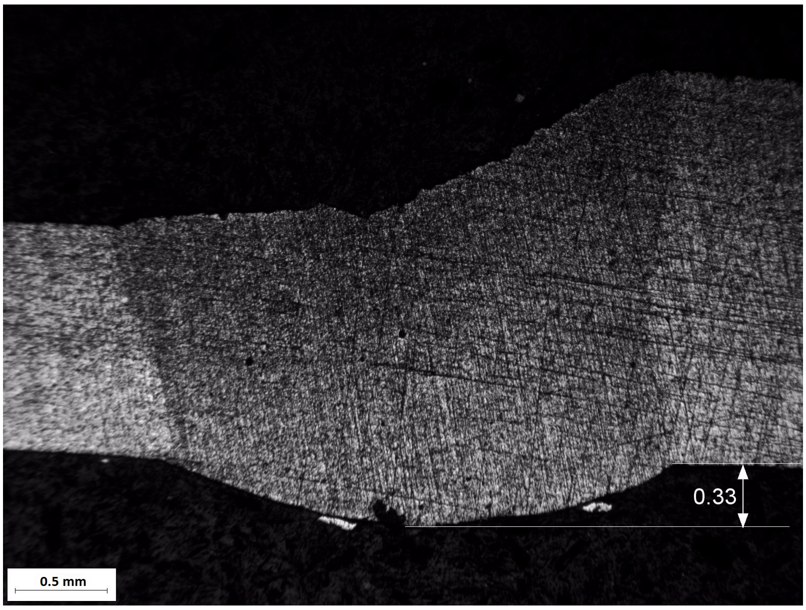


Figure 4.32: Ecessive root penetration defect in the specimen 6-03

*Negative mismatch*: As explained in the previous chapter, this type of defect leads to a weakening of the weld section. The specimens with this type of defect are: 6-04, 6-06, 6-08, 6-09.

Finally, it is noted that no specimen was found to have the *weld sagging* defect.

### 4.2.4 Tensile test results 6016 alloy

In the table 4.8 the results of the tensile test for the 6016 alloy specimens are reported, while in table 4.9 the means value, the standard deviation and the COV have been computed. It's evident how the 6016 showed better performance in the tensile test, with respect to the 5754 alloy. This behaviour could be explained by the fact that, despite the defects, all the joints were formed and all the material was fused. More than half specimens showed rupture on the base material of the thinner sheet (BM in the table), meaning a good mechanical resistance of the welded joint. In table 4.9 are highlighted in green the samples that have reported rupture on the base material. It can be seen that the COV values are quite low, a sign of the homogeneity of the weld seam along its length. Specimens 6-02 and 6-08 showed the lowest performance on the tensile test and the highest COV values, we remember how these two specimens were affected by an important porosity defect. Lastly, in the figure 4.33 the tensile test maximum load is showed in function of the Heat Input used during the welding process. The specimens that showed the optimal tensile load and the rupture have been obtained using a Heat Input HI = $7.21 \div 11.22\ J/mm$. It should be noted that this last remark does not specify what would be the optimal heat input to be used for this alloy, as it has been seen in the section on micrographs, as it is necessary to adjust the heat input to avoid some welding defects, but it is possible to have an idea of the range on which to move. The figure 4.34 shows an example of the curve obtained during the tensile test of the specimen 6-01, which underwent rupture on the base material of the thinnest sheet. It can be seen that after reaching the maximum load there is a short zone where the load decreases, a sign of a necking of the section of the test piece.

The figure 4.35 shows the curve obtained during the tensile test of the specimen 6-03, with rupture on the welded joint.

| Specimen | Test 1 | | Test 2 | | Test 3 | |
|---|---|---|---|---|---|---|
| | Crack | LOAD (N) | Crack | LOAD (N) | Crack | LOAD (N) |
| 6-01 | BM | 2845,7 | BM | 2784,5 | BM | 2822,9 |
| 6-02 | W | 2244,2 | W | 2262,5 | W | 2499,8 |
| 6-03 | W | 2749,2 | W | 2738,9 | W | 2806,8 |
| 6-04 | BM | 2981,0 | BM | 2944,8 | BM | 2923,2 |
| 6-05 | BM | 2834,9 | BM | 2838,5 | BM | 2841,1 |
| 6-06 | BM | 2861,5 | BM | 2843,8 | BM | 2849,5 |
| 6-07 | W | 2833,0 | BM | 2809,2 | BM | 2801,0 |
| 6-08 | W | 1803,4 | W | 2783,8 | W | 2731,4 |
| 6-09 | BM | 2787,8 | BM | 2815,4 | BM | 2819,0 |

Table 4.8: Maximum tensile load and point of rupture 6016 alloy

### 4.2.5 Erichsen cupping test results 6016 alloy

The results of the Erichsen cupping test are reported in the tables 4.10 and 4.11. The 6016 alloy specimens that returned the best results in the tensile test are: 6-01, 6-04, 6-05, 6-06 and 6-09. It is observed that most of these also reported good results in the Erichsen cupping test. Also in this case from the table 4.11 it is possible to observe a great dispersion of data. In the graph in figure 4.36 the results are plotted in function of the Heat Input (J/mm).

| Specimen | Mean (N) | Standard Deviation (N) | COV% |
|---|---|---|---|
| 6-01 | 2817,7 | 30,9 | 1,1 |
| 6-02 | 2335,5 | 142,6 | 6,1 |
| 6-03 | 2765,0 | 36,6 | 1,3 |
| 6-04 | 2949,7 | 29,2 | 1,0 |
| 6-05 | 2838,2 | 3,1 | 0,1 |
| 6-06 | 2851,6 | 9,1 | 0,3 |
| 6-07 | 2814,4 | 16,6 | 0,6 |
| 6-08 | 2439,5 | 551,6 | 22,6 |
| 6-09 | 2807,4 | 17,1 | 0,6 |

Table 4.9: Tensile load mean value, standard deviation and COV 6016 alloy

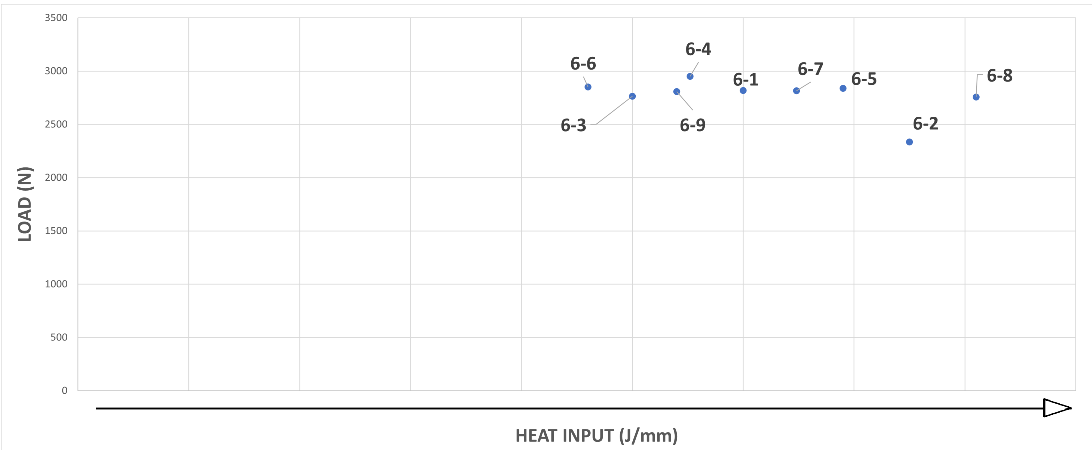


Figure 4.33: Tensile test results versus Heat Input 6016 alloy

| Specimen | Test 1 | | Test 2 | | Test 3 | |
|---|---|---|---|---|---|---|
| | Crack | EI (mm) | Crack | EI (mm) | Crack | EI (mm) |
| 6-01 | W | 2,2 | W | 3,2 | W | 3,6 |
| 6-02 | W | 2,2 | W | 1,6 | W | 3,3 |
| 6-03 | W | 1,4 | W | 2,8 | W | 2,8 |
| 6-04 | W | 3,5 | W | 3,2 | W | 3,0 |
| 6-05 | W | 3,3 | W | 3,4 | W | 3,5 |
| 6-06 | W | 2,7 | W | 3,6 | W | 3,2 |
| 6-07 | W | 3,6 | W | 3,1 | W | 3,6 |
| 6-08 | BM | 3,2 | BM | 3,4 | BM | 3,2 |
| 6-09 | W | 3,7 | W | 2,7 | W | 1,0 |

Table 4.10: Erichsen Index's and Point of rupture 6016 alloy

| Specimen | Mean (mm) | Standard Deviation (mm) | COV% |
|---|---|---|---|
| 6-01 | 3,0 | 0,7 | 23,0 |
| 6-02 | 2,4 | 0,8 | 35,8 |
| 6-03 | 2,3 | 0,8 | 35,4 |
| 6-04 | 3,3 | 0,2 | 7,2 |
| 6-05 | 3,4 | 0,1 | 3,1 |
| 6-06 | 3,2 | 0,5 | 15,3 |
| 6-07 | 3,4 | 0,3 | 7,8 |
| 6-08 | 3,3 | 0,1 | 4,1 |
| 6-09 | 2,5 | 1,4 | 54,5 |

Table 4.11: Erichsen Index's mean value, standard deviation and COV 6016 alloy

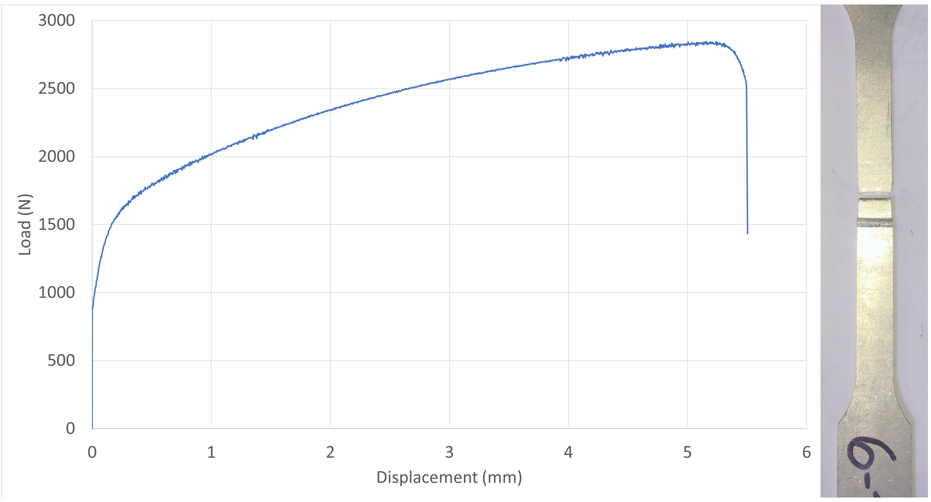


Figure 4.34: Tensile test curve specimen 6-01 with rupture on the base material

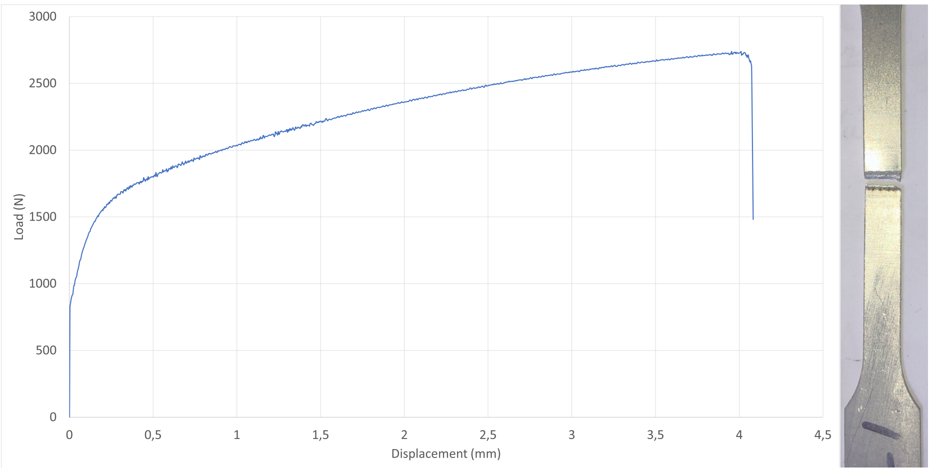


Figure 4.35: Tensile test curve specimen 6-03 with rupture on the welded joint

### 4.2.6 Summary of the result analysis 6016 alloy

The graph in the figure 4.37 shows the performance of the 6016 alloy specimens in the tensile test and in the Erichsen cupping test. Interestingly, there is not much difference between the different points in the graph, reporting very similar values of maximum load (N) and Erichsen's index (mm). Given this similarity in the results, one could consider as a discretizing factor the breakage in the base material in the tensile test: 6-1, 6-4, 6-5, 6-6, 6-9.

Considering the images obtained under the microscope of the cross-section of these specimens, it can be observed that these specimens present only the defect of excessive

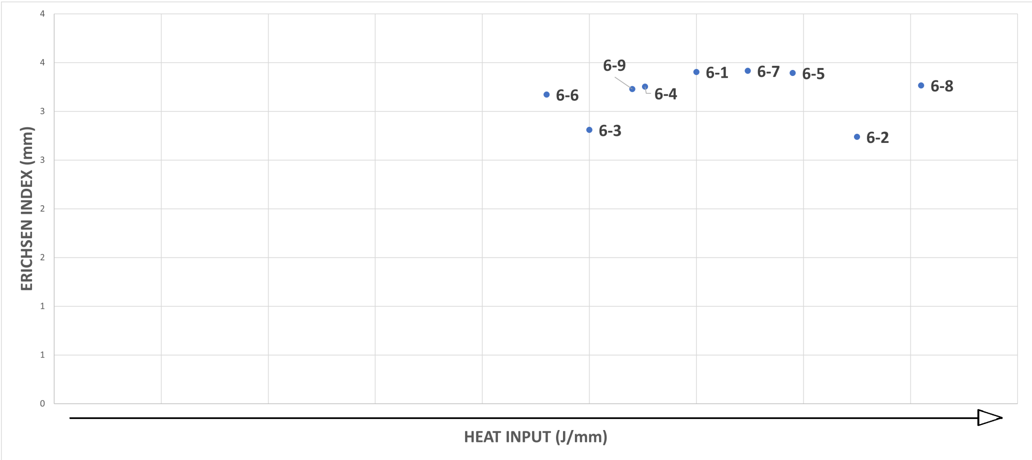


Figure 4.36: Erichsen test results versus Heat Input 6016 alloy

root penetration (apart from specimen 6-01 which also presents a hot crack defect).

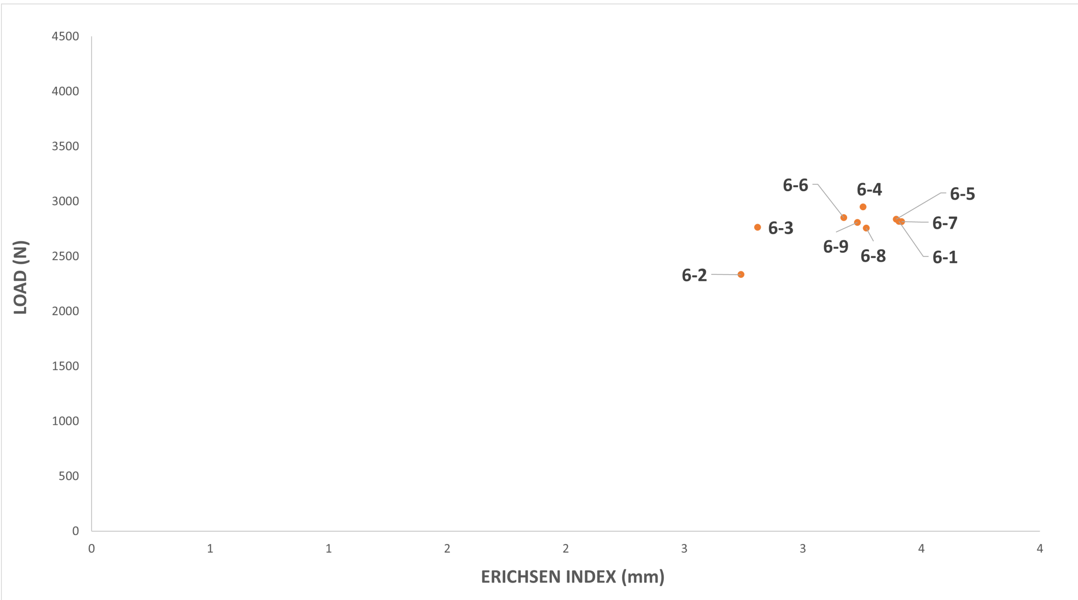


Figure 4.37: Maximum load versus Erichsen's index 6016 alloy

This defect, as already seen, can be solved by decreasing the thermal input. In the table 4.12 the values of Heat Input (J/mm) and Focal length (mm) of the considered specimens are reported. In this case it is difficult to find an optimal focal length, although it is always good to place the focus of the laser beam below both surfaces.

| Specimen | Heat Input HI (J/mm) | Focal length (Taguchi level) |
|---|---|---|
| 6-01 | 9.62 | 2 |
| 6-04 | 8.85 | 1 |
| 6-05 | 11.06 | 3 |
| 6-06 | 7.37 | 2 |
| 6-09 | 8.65 | 1 |

Table 4.12: Heat Input values for specimens 6-01, 6-04, 6-05, 6-06, 6-09

# Chapter 5

# Conclusions

## 5.1 General Summary

During this thesis work, an experimental analysis of the mechanical properties of Tailor Welded Blanks components, obtained by laser butt welding two sheets of the same alloy and of different thickness (2mm and 1.2mm), was performed. Two aluminum alloys from the 5xxx and 6xxx series were used: EN AW5754 and EN AW6016. An Nd:YAG laser was used to perform the welding operations and three process parameters were varied: power, weld speed, and focal length. Wanting to observe the influence that the single parameter has, but also the combination of the three, a DOE design of experiment was designated by using the *Taguchi* approach. This thesis is a counter-evidence and refinement of the extensive work done by another thesis student of the Politecnico di Torino, in fact, the DOE was programmed based on the results previously obtained. To characterize the welded joint, tensile tests, Erichsen cupping tests were performed, and the cross-section of the joint was observed under a microscope.

The results obtained can be summarized:

1. Achieving a high-quality joint requires a one-pass weld. In fact, you can ensure complete fusion of the material by choosing the correct welding parameters. It has been seen how the use of multiple passes leads to the generation of welding defects such as: porosity, positive misalignment and negative misalignment;

2. Observing the cross-sections of the joints under a microscope and comparing them with the literature it has confirmed that the factor most influencing the size of the weld cross-section is the focal distance. In fact, this must be chosen in such a way as to point the laser beam below both metal sheets, so as to guarantee correct heat diffusion;

3. In the previous thesis work, shielding gas was used during welding, using a He (helium) flow rate of 15 l/min, in contrast to the current work, where no shielding gas was used. In the EN AW6016 alloy, the non-use of helium led to the use of higher laser powers to achieve a well-formed joint. In EN AW5754 alloy, the non-use of shielding gas led to welding defects;

4. The influence of heat input on the welding of sheets of different thicknesses has been identified, finding for both alloys a potential range of heat input which, combined with a correct shielding gas flow rate, can lead to the formation of a good welding joint;

5. Modification of the fixing system previously used resulted in lower sheet misalignment defects;

6. The Taguchi model analysis did not produce statistically significant results. This may be due to the fact that we used too narrow a range of parameters around an optimal set already identified in previous work.

## 5.2 Recommendations for future research

A first recommendation for future research developments might be to focus the study on a single alloy. Since, in fact, laser welding on aluminum alloys is a process in full evolution, it is not easy to keep track of all the parameters that influence this process. To properly execute a new testing campaign, starting with the parameters mentioned in the following thesis, it will be necessary to:

- select and use a flow rate of He as shielding gas (15 l/min could be a reasonable value);

- always use the same incidence angle during the welding process, so that it is easily repeatable: an angle of 20 degrees with respect to the vertical seems to have produced good results;

- ensure a perfectly symmetrical cut of the specimens to be used for the Erichsen cupping test, so as to minimize data dispersion;

Finally, a future development of the study could be to use weld simulation software (e.g. *Sysweld*), and develop a FEM model of the welding process by performing a thermomechanical analysis.

# Bibliography


[1] UNI EN 10359:2015. Profili saldati al laser (tailored blanks) - condizioni tecniche di fornitura. 2012-11.

[2] Katayama S (2012). Laser welding of aluminum alloys. *Journal of Japan Institute of Light Metals*, 2012.

[3] ISO 20482:2013. Metallic materials — sheet and strip — erichsen cupping test. 2012-11.

[4] ISO 4136:2012. Destructive tests on welds in metallic materials — transverse tensile test. 2012-11.

[5] Behrouz Bagheri, Mahmoud Abbasi, and Reza Hamzeloo. Comparison of different welding methods on mechanical properties and formability behaviors of tailor welded blanks (twb) made from aa6061 alloys. *Proceedings of the Institution of Mechanical Engineers, Part C: Journal of Mechanical Engineering Science*, 235(12):2225–2237, 2021.

[6] K. Y. Benyounis and A. G. Olabi. Optimization of different welding processes using statistical and numerical approaches - a reference guide. *Adv. Eng. Softw.*, 39(6):483–496, jun 2008.

[7] Simone Bergamo. Saldatura laser su leghe di alluminio: studio delle proprietà meccaniche e microstrutturali. *[Master's Thesis, Politecnico di Torino]*, 2021.

[8] E. Brünger, Olaf Engler, and Juergen Hirsch. *Al-Mg-Si sheet for autobody application*, pages 51–61. 10 2006.

[9] Marcello Cabibbo, Chiara Paoletti, Mohamed Ghat, Archimede Forcellese, and Michela Simoncini. Post-fsw cold-rolling simulation of ecap shear deformation and its microstructure role combined to annealing in a fswed aa5754 plate joint. *Materials*, 12(9), 2019.

[10] X. Cao, W. Wallace, J.-P. Immarigeon, and C. Poon. Research and progress in laser welding of wrought aluminum alloys. ii. metallurgical microstructures, defects, and mechanical properties. *Materials and Manufacturing Processes*, 18(1):23–49, 2003.

[11] X. Cao, W. Wallace, C. Poon, and J.-P. Immarigeon. Research and progress in laser welding of wrought aluminum alloys. i. laser welding processes. *Materials and Manufacturing Processes*, 18(1):1–22, 2003.

[12] G. Casalino, M. Mortello, P. Leo, K.Y. Benyounis, and A.G. Olabi. Study on arc and laser powers in the hybrid welding of aa5754 al-alloy. *Materials & Design*, 61:191–198, September 2014.

[13] Marco Cavazzuti. *Optimization Methods, From Theory to Design Scientific and Technological Aspects in Mechanics*. Springer, Berlin, Heidelberg, 2013.

[14] D.Narsimhachary. Effect of laser welding parameters on 6061 aluminium alloy. *Doctoral Thesis, Department of metallurgical institute of technology Rourkela Odisha*, 2014.

[15] Janet Folkes. Waterjet—an innovative tool for manufacturing. *Journal of Materials Processing Tech.*, 209(20):6181–6189, 2009.

[16] Tomas Forsman. Laser welding of aluminium alloys. *Doctoral Thesis, Department of Materials and Manufacturing Engineering Division of Manufacturing Systems Engineering*, 2000.

[17] P. A. Friedman and G. T. Kridli. Microstructural and mechanical investigation of aluminum tailor-welded blanks. *Journal of Materials Engineering and Performance*, 9(5):541–551, October 2000.

[18] Peter Friedman and G. Kridli. Microstructural and mechanical investigation of aluminum tailor-welded blanks. *Journal of Materials Engineering and Performance*, 9:541–551, 01 2000.

[19] Niemann G. *Elementi di Macchine*. ETS. Springer, 1983.

[20] Seyed Hamidinejad, Mohammad Hasanniya, Nooshin Salari, and E. Valizadeh. Co2 laser welding of interstitial free galvanized steel sheets used in tailor welded blanks. *The International Journal of Advanced Manufacturing Technology*, 64, 01 2012.

[21] Kleinert H. Bräunling R. Jansen I. Häßler and Liebrecht. Patchworkkleben– partielle verstärkung von blechbauteilen für fahrzeuge. *Schindel-Bidinelli,E. (Ed.), Proceedings of the 17th International Symposium Swiss Bonding. Rap-perswil, Switzerland*, 896:141–154, 2003.

[22] M. Jie, C. H. Cheng, Luen Chow Chan, C. L. Chow, and Chak Yin Tang. Experimental and theoretical analysis on formability of aluminum tailor-welded blanks. *Journal of Engineering Materials and Technology, Transactions of the ASME*, 129(1):151–158, January 2007.

[23] N. KARUNAKARAN and V. BALASUBRAMANIAN. Effect of pulsed current on temperature distribution, weld bead profiles and characteristics of gas tungsten arc welded aluminum alloy joints. *Transactions of Nonferrous Metals Society of China*, 21(2):278–286, 2011.

[24] S. Katayama. Introduction:fundamentals of laser welding. In Seiji Katayama, editor, *Handbook of Laser Welding Technologies*, Woodhead Publishing Series in Electronic and Optical Materials, pages 3–16. Woodhead Publishing, 2013.

[25] Marion Merklein Maren Johannes Michael Lechner Andreas Kuppert. A review on tailored blanks—production, applications and evaluation. *[Journal of Materials Processing Technology]*, 214:151–164, 2014.

[26] M. KUTSUNA. Study on hot cracking in laser welding oj aluminium alloys. *IIW Doc IV*, pages 631–95, 1995.

[27] Muneharu Kutsuna. Metallurgical aspects in laser welding of steels and aluminum alloys. *International Congress on Applications of Lasers & Electro-Optics*, 1996(1):D122–D131, 1996.

[28] Ceyhun Köse. Laser weldability of 5754 aluminum alloy. *e-Journal of New World Sciences Academy*, 1:225–236, 09 2016.

[29] STANNER R. J. L. American scientist. vol 64 258. 1976.

[30] Liu, Jun, Gao, Haoxiang, El Fakir, Omer, Wang, Liliang, and Lin, Jianguo. Hot stamping of aa6082 tailor welded blanks: experiment and fe simulation. *Manufacturing Rev.*, 3:8, 2016.

[31] Andrea Casaroli Marco V. Boniardi. L'alluminio e le sue leghe. *[Dipartimento di Meccanica, Politecnico di Milano]*, 2013.

[32] W. Miao and David Laughlin. Effects of cu content and preaging on precipitation characteristics in aluminum alloy 6022. *Metallurgical and Materials Transactions A*, 31:361–371, 04 2012.

[33] Minitab. Support manual.

[34] Löwen Nagel M., Fischer R. and Straube O. Production and application of aluminum tailored blanks. *Proceedings of IBEC'97*, pages 87–91, 1997.

[35] Lung-Kwang Pan, Che-Chung Wang, Ying Hsiao, and Kye Ho. Optimization of nd:yag laser welding onto magnesium alloy via taguchi analysis. *Optics & Laser Technology*, 37:33–42, 02 2005.

[36] C Peister, R George, K Omer, M J Worswick, S Malcolm, J Dykeman, C Yau, R Soldaat, and W Bernert. Forming of an axially tailored automotive channel section through hot stamping of tailor-welded blanks. *Journal of Physics: Conference Series*, 896:012052, sep 2017.

[37] Stefan Pogatscher, H. Antrekowitsch, and Peter Uggowitzer. Interdependent effect of chemical composition and thermal history on artificial aging of aa6061. *Acta Materialia*, 60:5545–5554, 09 2012.

[38] Dausinger F. Rapp J. and Hugel H. Laser beam welding of aluminium alloys. *ECLAT'96*, pages 97–106, 1996.

[39] Uwe Reisgen, Markus Schleser, Oleg Mokrov, and Essam Ahmed. Optimization of laser welding of dp/trip steel sheets using statistical approach. *Optics & Laser Technology*, 44:255–262, 02 2012.

[40] R.K. Roy. *A Primer on the Taguchi Method*. VNR competitive manufacturing series. Society of Manufacturing Engineers, 1990.

[41] Katayama S. New development in laser welding. *New Developments in Advanced Welding*, 2005.

[42] Katayama S. Understanding and improving process control in pulsed and continuous wave laser welding. *Advances in Laser Materials Processing – Technology, Research and Applications*, 2010.

[43] Katayama S. 'laser welding', ferrum. *Bulletin of the Iron and Steel Institute of Japan*, 2012.

[44] Asiful Hossain Seikh, Ashfaq Mohammad, El-Sayed M. Sherif, and Abdulrahaman Al-Ahmari. Corrosion behavior in 3.5% nacl solutions of $\gamma$-tial processed by electron beam melting process. *Metals*, 5(4):2289–2302, 2015.

[45] H.R. Shakeri, A. Buste, M.J. Worswick, J.A. Clarke, Frank Feng, M. Jain, and M. Finn. Study of damage initiation and fracture in aluminum tailor welded blanks made via different welding techniques. *Journal of Light Metals*, 2:95–110, 05 2002.

[46] Yuliang Shi, Ping Zhu, Libing Shen, and Zhongqin Lin. Lightweight design of automotive front side rails with twb concept. *Thin-walled Structures - THIN WALL STRUCT*, 45:8–14, 01 2007.

[47] K Shibata, T Iwase, H Sakamoto, M Kasukawa, K Chiba, and H Saeki. Welding of aluminium tailored blanks by nd: Yag lasers. *Welding International*, 17(4):282–286, 2003.

[48] Przemysław Snopiński, Tomasz Tański, Klaudiusz Gołombek, Stanislav Rusz, Ondřej Hilser, Tibor Donič, Paweł M. Nuckowski, and Marcin Benedyk. Strengthening of aa5754 aluminum alloy by drece process followed by annealing response investigation. *Materials*, 13(2):301, Jan 2020.

[49] Przemysław Snopiński, Tański Tomasz, Klaudiusz Gołombek, Stanislav Rusz, Ondřej Hilšer, Tibor Donič, Paweł Nuckowski, and Marcin Benedyk. Strengthening of aa5754 aluminum alloy by drece process followed by annealing response investigation. *Materials*, 13:301, 01 2020.

[50] Sai AdityaPradeep Rakesh K.Iyer HakanKazan SrikanthPilla. Automotive applications of plastics: Past, present, and future. *[Applied Plastics Engineering Handbook (Second Edition)]*, pages 651–673, 2017.

[51] Guangyong Sun, Tong Pang, Chenglong Xu, Gang Zheng, and Jie Song. Energy absorption mechanics for variable thickness thin-walled structures. *Thin-Walled Structures*, 118:214–228, 2017.

[52] Gaute Svenningsen, Magnus Hurlen Larsen, Jan Halvor Nordlien, and Kemal Nisancioglu. Effect of high temperature heat treatment on intergranular corrosion of almgsi(cu) model alloy. *Corrosion Science*, 48:258–272, 2006.

[53] D.S. ; Totten, G.E.; Mackenzie. *Handbook of Aluminum: Physical Metallurgy and Processes, volume 1*. Gallimard, 2003.

[54] Manjunath Viswabrahmana and A.V. Suresh. Experimental investigation of tubular crushing and tubular bending of twb application in automotive vehicles for frontal crash. *Materials Today: Proceedings*, 2021.

[55] Xiang-Jie Wang, Wei Sun, Jun-Fu Chen, Fu-Yue Wang, Lei Li, and Jian-Zhong

Cui. Microstructures and properties of 6016 aluminum alloy with gradient composition. *Rare Metals*, 40, 08 2020.

[56] Wuhua Yuan and Zhenyu Liang. Effect of zr addition on properties of al–mg–si aluminum alloy used for all aluminum alloy conductor. *Materials & Design - MATER DESIGN*, 32:4195–4200, 09 2011.

[57] Hao Zhong, P.A. Rometsch, and Yuri Estrin. Effect of alloy composition and heat treatment on mechanical performance of 6xxx aluminum alloys. *Transactions of Nonferrous Metals Society of China*, 24:2174–2178, 07 2014.

[58] Babić Ž and Milan Šljivić. Application of tailored blanks in the automotive industry. volume 27, 12 2002.